NONLINEAR PERMEABILITY OF COMPOSITES FOR NONLINEAR TRANSMISSION LINES AT MICROWAVE FREQUENCIES

by

Travis D. Crawford

A Thesis

Submitted to the Faculty of Purdue University

In Partial Fulfillment of the Requirements for the degree of

Master of Science in Nuclear Engineering

School of Nuclear Engineering

West Lafayette, Indiana

December 2020

THE PURDUE UNIVERSITY GRADUATE SCHOOL

STATEMENT OF COMMITTEE APPROVAL

Dr. Allen Garner, Chair

School of Nuclear Engineering

Dr. Robert Bean

School of Nuclear Engineering

Dr. Tyler Tallman

School of Aeronautics and Astronautics

Approved by:

Dr. Shripad Revankar

To my family

ACKNOWLEDGMENTS

Science is a collaborative effort both in the lab and in the home. As such, I would be remiss to think that this work was done entirely on my own accord. There are many who deserve credit for the success of this research and as such, I shall try my best to make their efforts known.

Mom, Dad, Amanda, Garrett, and Brandon, thank you for your constant support over the years, especially in the last two when I needed it most. I am truly fortunate and humbled to be able to call you all family.

Keri, thank you for keeping me sane. For giving me a reason to leave the lab and giving me something to look forward to come home to.

James, Zinn, Naj, Chuck, and the rest back home, thank you for the laughs and friendship. Even though we are thousands of miles away from each other, your support means the world to me.

Coach Donnelly, even though you're no longer with us, thank you for the many life lessons you taught me. They truly helped me get through some of the tougher days of graduate school.

Aunt Hazel and Jim Singer, thank you for your support and willingness to help me chase my goals.

Dr. Allen Garner, thank you for your genuine support and advice. For being real with your students. For your determination in helping your graduate students get funding. For being passionate about what it is you do, even when your students sometimes make it hard.

Andrew and Russ, thank you for just being genuine standup dudes. For your guidance and friendship and for showing me graduate school is more then just work, even when it doesn't feel like it.

Lastly, thank you to all the members of BEEP lab who have aided in this work both indirectly and directly. A special thanks to Jeremy and Xiao for their efforts as well.

This work was supported by the Office of Naval Research under Grant No. N000014-18-1-2341.

TABLE OF CONTENTS

LIST OF TABLES

LIST OF FIGURES

ABSTRACT

Nonlinear transmission lines (NLTLs), which exhibit permittivity as a function of electric field and/or permeability as a function of magnetic field strength, are of increasing importance for sharpening pulses to less than 100 ps and serving as radiofrequency (RF) sources; however, NLTLs often are not easily modified to achieve different output parameters. One method under investigation involves combining inclusions of nonlinear dielectric (barium strontium titanate (BST)) and/or magnetic (nickel zinc ferrite (NZF)) inclusions to tune NLTL properties by adjusting inclusion loading fractions. This thesis focuses on measuring the nonlinear permeability and magnetic loss tangent of composites comprised of various volume loadings of NZF or a combination of NZF and BST inclusions encapsulated in a silicon matrix. We measured the relative permeability from 1 - 4 GHz using a coaxial airline while biasing the samples in an external DC magnetic field from 0 – 171 kA/m. The permeability decreased from 1 to 4 GHz for each volume fraction but increased with increasing magnetic field strength at low magnetic field strengths with sufficient NZF volume loading. The magnetic loss tangents of the composites increased with increasing frequency and/or NZF volume fraction but were suppressed by increasing the external magnetic field strength. Adding BST to an NZF composites did not cause a significant change in permeability compared to NZF alone, based on an analysis of variance (ANOVA) and multiple comparison test. These results elucidate the frequency, magnetic field, and volume loading dependence of NZF at microwave frequency and provide initial information for simulating NLTLs and examining more comprehensive RF system behavior.

We then investigated the feasibility of tapering the NLTL by modifying the inclusion loading down the line to control the device's electric and magnetic properties to achieve greater system flexibility and rigidity. Unlike conventional tapering by gradually changing the line size, this method bypasses the complex, difficult to manufacture geometries by leveraging the experimental results obtained for our NZF and BST composites. Potential drawbacks of extending this approach to nonlinear materials and NLTLs is discussed.

1. INTRODUCTION

Over the past century, the volatile landscape of the electronic industry has brought forth the extensive development of directed energy systems. The directed energy community is typically divided between lasers and high power microwave (HPM) systems. HPM systems are deeply rooted in applications such as communication, fusion heating, RADAR, electronic warfare, and non-lethal weapons [4]. Vacuum devices have dominated the HPM market for the last century giving rise to extensive development of electron-beam devices, gyrotrons, klystrons, Backward Wave Oscillators (BWOs), and Traveling Wave Tubes (TWTs) [4],[5]. While the technology for these devices is well established and advanced, complicated geometries coupled with the necessity of a vast array of auxiliary systems make HPM vacuum devices cumbersome and vulnerable to system failure, making them unpractical in situations where system rigidity is necessary [5][6].

Nonlinear Transmission Lines (NLTLs) are increasingly viewed as alternatives to the aforementioned vacuum HPM devices. NLTLs are designed to be compact, tunable, solid state HPM devices, making them more attractive as the HPM source within a directed energy system. While NLTLs can take on many topologies, their production of radio frequency (RF) is governed by the inverse relation between the nonlinear permittivity and/or permeability and the phase velocity of an incident pulse, given by $v_p = c/[\epsilon_r(V)\mu_r(I)]^{-1/2}$ [7][8]. As the pulse propagates down the line, the crest of the pulse is forced to propagate faster than the base, leading to sharpened rise- and fall-times [7][9]. In several experiments, NLTLs have achieved rise times on the order of hundreds of picoseconds making them attractive from a pulse sharpening and microwave generation perspective [10][8]. Sufficient sharpening inevitably leads to the formation of an electromagnetic shockwave within the line, resulting in oscillations induced by the motion of a material's magnetic moment and/or dipole [10].

To fully develop the motivation for our research, we first discuss the fundamentals of the different NLTL topologies along with a review of magnetization dynamics in Chapter 2. Following this, we discuss our experimental methods and results in Chapter 3 followed by a discussion on impedance tapering in Chapter 4. Concluding remarks are made in Chapter 5.

2. BACKGROUND

The realization of RF generation using NLTLs has led to the development and implementation of several NLTL topologies. Broadly speaking, NLTLs may be divided into two categories: lumped element and gyromagnetic. Within both these two categories exists another type of NLTL referred to as a Hybrid NLTL, which simply implies both nonlinear permeability and permittivity are being used as opposed to just one or the other. A brief discussion of each topology is given to motivate our research.

2.1 Lumped Element Lines

Unlike other geometries, lumped element NLTLs advantageously have allowed for the rigorous development of NLTL theory through circuit analysis and simulation. These systems can be represented as abacuses of nonlinear inductors and/or capacitors as shown in figure 1.

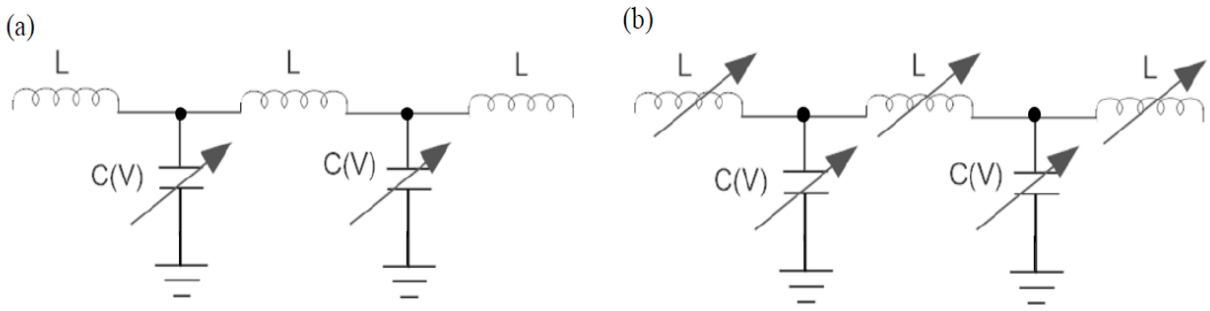

Figure 1(a) Lumped element NLTL with nonlinear capacitors and (b) both nonlinear capacitors and inductors, typically referred to a hybrid line. ©2018 IEEE [11]

Wave propagation theory through nonlinear and linear media has been well developed since the mid-20th century. Ultimately, the wave equation for the circuit is derived from Kirchhoff's laws for whichever nonlinear component is used. For example, in [12], the wave equation developed from a KVL and KCL analysis of a lumped element NLTL with nonlinear capacitance is given by (1) where we see that one recovers the linear transmission line equation if the capacitance is constant.

$$L\frac{\partial}{\partial t}\left(C(V)*\frac{\partial V}{\partial t}\right)=\frac{\partial^2 V}{\partial x^2} \quad (1)$$

Along with the mathematical theory development, lumped element NLTLs also lend themselves to convenient experimental design and can be built with commercial off-the-shelf-devices [10][13]. Several experimental studies with lumped element NLTLs containing nonlinear inductors, capacitors, or both nonlinear capacitors and inductors have shown good agreement with models [10] [14]. One drawback of lumped element NLTLs is the frequency of the RF generated. In nonlinear capacitance lines, due to the mechanism of RF generation, studies [13][16] reported average frequencies in the low MHz with combinations of nonlinear inductors and capacitors reaching high MHz [15]. Lines using nonlinear inductors have achieved low GHz frequencies; however, the total line length makes these systems impractical for field deployment [5].

2.2 Gyromagnetic NLTLs

Gyromagnetic NLTLs employ nonlinear magnetic materials, such as ferrites, that induce microwave oscillations due to the motion of the material's magnetic moments [7][9]. These devices are typically manufactured in a coaxial geometry with toroidal ferrites wrapped around the center conductor, as shown in figure 2. An insulating material, such as SF_6, Sylgard 184, or EFI, is typically placed between the outer conductor and ferrite/inner conductor to prevent breakdown [4]. Gyromagnetic NTLS's are often biased in an external magnetic field by permanent magnets or a solenoid to allow for coherent precession [7]. Further discussion on the physics of this mechanism is given in the following section on magnetization dynamics.

In practice, gyromagnetic NLTLs have shown promising results. Several groups have produced peak RF powers in the hundreds of MW in the low GHz regime [7][9]. Several experiments have integrated gyromagnetic lines into phased array systems by biasing the ferrites at different DC magnetic fields [17][18]. One experiment successfully beam steered a 4-element NLTL array by manipulating the biasing field to achieve output powers of 4MW with frequency

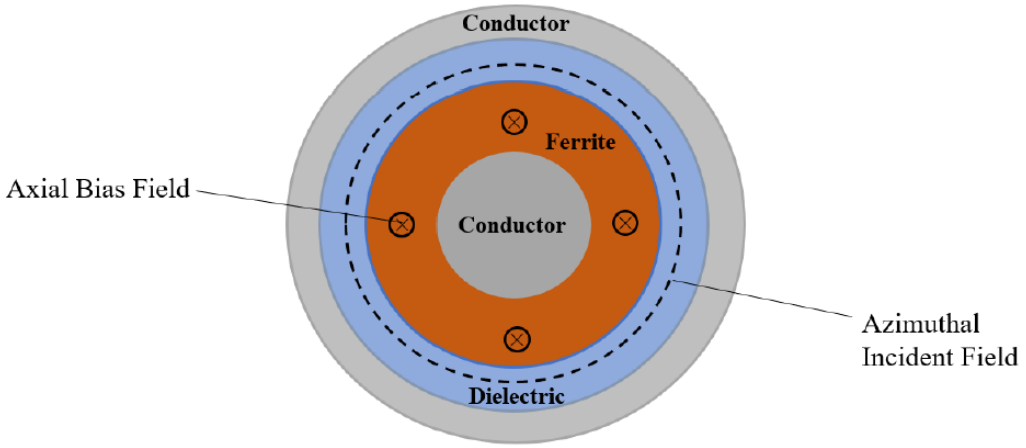

Figure 2 An example of a cross section of gyromagnetic NLTL. The center conductor is surrounded by ferrite while an insulating dielectric between the ferrite and outer conductors.© 2013 IEEE[7]

agility of 2-4GHz [10][17]. These lines typically have higher efficiencies in comparison to the lumped element lines making them more appealing [19]. For example, in [53]-[55], lumped element NLTLs had RF conversion efficiencies of 10, 7, and 12%, respectively whereas biased gyromagnetic lines in [56] had conversion efficiencies of 20%.

2.3 Hybrid Nonlinear Transmission Lines

A hybrid nonlinear transmission line is a transmission line which leverages both of the aforementioned nonlinear mechanisms in a single system. In practice, these types of lines can take the form of both lumped element and coaxial geometries although the implementation of the nonlinear components is different.

Lumped element hybrid lines consist of the combination of nonlinear capacitors and inductors. Experimentally, few groups have investigated this type of line however, circuit simulation software such as SPICE have been used to model the effects of having both nonlinear components. For example, one study used SPICE simulations to model a hybrid line by using varactor diodes as nonlinear capacitors and nonlinear inductors modeled from proprietary ferrites[57],[10]. Alternatively, others have built lumped element hybrid lines using commercial

off the shelf components achieving frequencies in the low MHz with peak output powers of 5kW[10],[58].

In contrast, hybrid nonlinear transmission lines implementing the coaxial topology can leverage nonlinear bulk materials. Such a line would consist of ferroelectric and ferrimagnetic materials such as barium titanate or barium strontium titanate in conjunction with some ferrite surrounding the center conductor of the line. Since ferroelectric materials generally produce lower frequency oscillations but ferrimagnetic materials are a greater risk for generating breakdown, a line consisting of both materials may have over all material properties which are more desirable than the single nonlinear material case [10]. Such a line is the motivation for the development of the composites discussed in this thesis.

2.4 Magnetism Fundamentals

Recall that from Maxwell's equations that magnetism is not due to the existence of magnetic monopoles, but rather due to the movement of electric charges [20]. Moreover, the physical property of electron spin along with the orbit of the electron around the nucleus permits the analogy of a closed Amperian loop of current. As such, the closed loop has an associated magnetic field, giving rise to the notion of a magnetic dipole shown in figure 3. The orientation and strength of the magnetic dipole is represented by the vector quantity known as the magnetic dipole moment, or magnetic moment for short, given by

$$\mathbf{m} = \mu_o \mathbf{I} S, \tag{2}$$

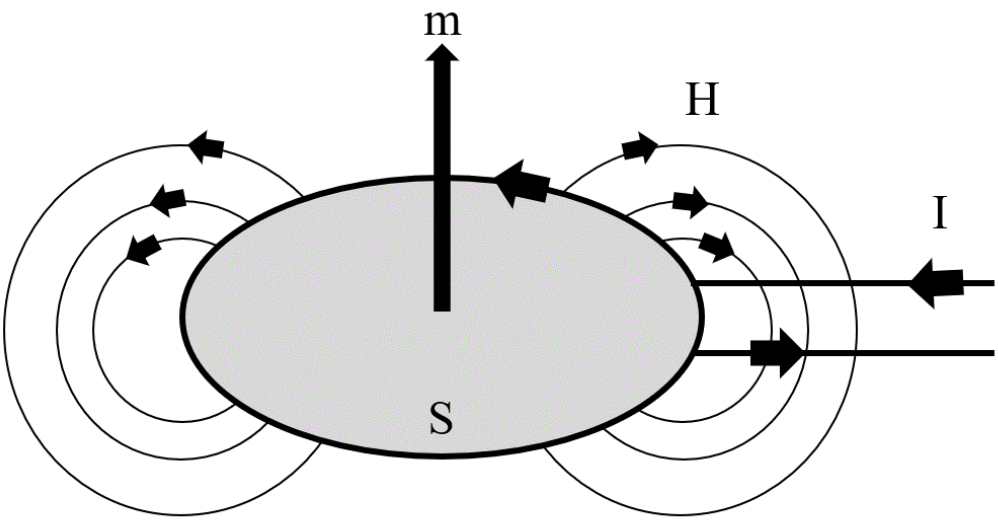

Figure 3. Illustration of magnetic moment $\vec{m}$ from a current loop with current *I* and area *S*.

where *I* is the current, *S* is the area, and μ_o is the permeability of free space. Using constitutive relations for the current and realizing that the orbiting electron also has an associated angular momentum due to its mass, the magnetic moment and the electron angular momentum may be related by [21][4]

$$\mathbf{m} = \frac{q\mu_o}{2m_e}\mathbf{L}, \tag{3}$$

where q is the electron charge, m_e is the electron mass, and **L** is the angular momentum. Since we are more interested in the moment's behavior when perturbed and since a magnetic moment in an external magnetic field experiences a change in angular momentum, or torque, given by $\mathbf{m} \times \mathbf{H}$, (3) may be recast by taking the derivative and applying the constitutive relation for the change in angular momentum to obtain

$$\frac{d\mathbf{m}}{dt} = -\gamma(\mathbf{m} \times \mathbf{H}), \tag{4}$$

where

$$\gamma = g\frac{q\mu_o}{2m_e}. \tag{5}$$

where g is the Lande factor, which is a quantum mechanically derived correction factor whose formulation is beyond the scope of this thesis [22].

While (4) suggests that the magnetic moment will precess forever about a magnetic field, we know this not to be the case in reality. In the mid-20th century, Landau, Liftshitz, and Gilbert developed the LLG equation for magnetization dynamics, which added a dampening term to (3) to account for the alignment of the moment with the applied field. The LLG equation is given by [7]

$$\frac{\partial \mathbf{m}}{\partial t} = -\gamma(\mathbf{m} \times \mathbf{H}) + \left(\alpha \mathbf{m} \times \frac{\partial \mathbf{m}}{\partial t}\right), \tag{6}$$

where the first term on the right-hand side (RHS) expresses the precession of the moment about the effective magnetic field, the second term on the RHS describes the dampening, and α is the dampening constant that depends on the material under analysis and typically varies between 0.01-1 [7].

The sum of all the individual magnetic moments over a volume is known as the magnetization **M**. Usually, all a material's magnetic moments are randomly oriented such that the net magnetization of the material is zero. In general, most material's moments weakly interact with an external field, leading to very small **M**. Such materials are paramagnetic, where their moments try to align parallel to the field, or diamagnetic, where their moments align slightly antiparallel [20]. However, in ferrous material, the magnetic moments exist within the confines of domain walls [20]. Each moment within the domain tends to point in the same direction as its neighbor, leading to larger net moments on the macroscopic level. Applying an external field causes these domains to strongly align with the applied field, leading to a large net magnetization. When a field of sufficient strength is removed, the domains of ferrous materials retain information about the applied field and remain aligned in position until brought to the Curie temperature or exposed to a field of opposite polarity [20]. Such a phenomenon is known as hysteresis and is best understood by graphing the magnetic auxiliary, or applied, field *H* versus the magnetic flux density *B* as shown in figure 4.

In general, there are several points of note on a hysteresis curve. Starting at the origin, when an external magnetic field *H* is applied to the sample, the magnetic flux density increases as seen in figure 4. Eventually, when a field is applied of sufficient strength, the sample becomes

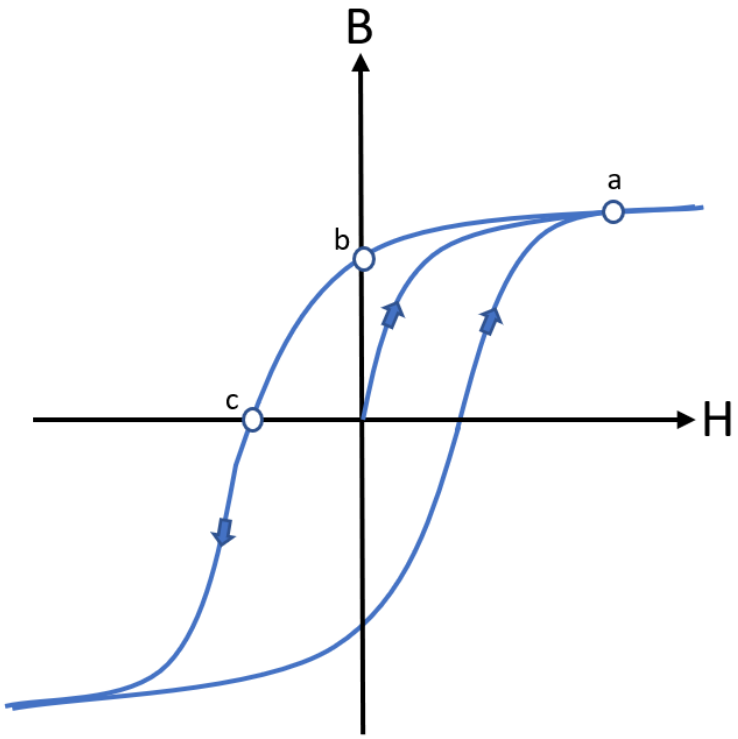

Figure 4 The hysteresis loop for a typical ferrite. The saturation point is denoted by *a*, the retentivity is denoted by *b*, and the coercivity is denoted by *c*.

magnetically hard or saturated and the flux density no longer increases. When the applied field is removed, the sample remains in a magnetized state and as such retains information about the field applied. This is known as the retentivity of the material as some remnant magnetization still exists. To remove this remnant magnetization, a field of opposite polarity is needed to coerce the magnetic moments such that the flux density is equal to zero. This point is known as the coercivity of the material. The same phenomenon continues when a field of opposite polarity is applied resulting in a loop known as the hysteresis loop of the material.

The realization of different materials reacting differently to magnetic fields led to the development of the definition of a material's permeability, an intrinsic property of a material that

describes its degree of magnetization. Ferrous materials tend to have large permeability and thus their magnetic moments are very responsive to an applied field resulting in a large net magnetization. In the context of gyromagnetic NLTLs and as previously mentioned, the generation of microwave oscillations depends on the damped gyromagnetic precession of the material's magnetic moments. This mode of microwave oscillation makes ferrites the material of choice since their large permeability indicates that their magnetic moments are highly responsive to a magnetic field or, analogously, a current pulse.

3. EXPERIMENTS

3.1 Introduction to Experiments

Nonlinear transmission lines (NLTLs) offer a robust, solid state solution for generating high power microwaves (HPM). Unlike conventional vacuum microwave sources, NLTLs employ nonlinear materials whose dielectric and/or magnetic properties vary with voltage and/or current, respectively, to modulate a delivered pulse [10],[23],[24]. Geometry and material selection can greatly impact NLTL performance, motivating material development and characterization at microwave frequencies. Nonlinear materials, such as barium strontium titanate (BST) and nickel zinc ferrite (NZF), are used in various NLTL topologies for their nonlinear permittivity and permeability, respectively [10],[25]. Both materials, albeit by different means, aid in generating an electromagnetic shockwave governed by the inverse relationship between phase velocity and the material's permeability and permittivity. In ferrite based lines, often called gyromagnetic lines, the propagation of the shockwave results in the dampened gyromagnetic precession of the material's magnetic moments around the effective magnetic field [7],[9],[10]. Gyromagnetic NLTLs often bias nonlinear ferrimagnetic material in an external magnetic field to allow for coherent precession of the magnetic moments. This can increase the peak output power of the system and generate sharper rise-times [7].

The motion of the magnetic moment **m** is described by the normalized Landau-Lifshitz-Gilbert (LLG) equation, given by [7]

$$\frac{\partial \mathbf{m}}{\partial t} = (-\gamma \mathbf{m} \times \mathbf{H_{eff}}) + \left(\alpha \mathbf{m} \times \frac{\partial \mathbf{m}}{\partial t}\right) \quad (7)$$

where the first term describes the precession of the moment about the effective field $\mathbf{H_{eff}}$ with γ the gyromagnetic factor, and the second term describes the dampening with α the dampening constant.

Unlike ferrites, it is hypothesized that BST generates microwaves by exploiting the titanate's crystalline structure [24]. When in a ferroelectric state, the titanate's structure permits the formation of a permanent dipole [24],[10], which is removed when the structure is brought to the Curie temperature and enters a paraelectric state [24]. The oscillation of the dipole moments

between the ferroelectric and paraelectric states is hypothesized to produce the microwave oscillations.

Combinations of ferroelectric materials and ferrites have been explored for various applications. For example, ferrite cores in high energy density capacitors were coated with barium titanate to increase the permittivity of the capacitors [25]. Other studies have shown that adjusting volume fraction, inclusion aspect ratio, and inclusion shapes facilitated the tuning of the material's electromagnetic properties [3],[26],[27]. Similarly, manipulating the volume fractions of BST and NZF inclusions will permit the adjustment of a composite's bulk permittivity and permeability [28].

Composites containing nickel zinc ferrite have been developed in numerous studies [59]-[63]. However, their nonlinear behavior is seldom measured and discussed in the context of application to NLTLs. Moreover, the combination of materials presented here has implications on the development of hybrid NLTLs that utilize both ferroelectric and ferrimagnetic bulk materials [3]. While characterizing the material's nonlinear behavior is paramount for NLTL systems, these prior studies have only considered material in the nonlinear regime at sub-GHz frequencies or the linear regime at microwave frequencies. Implementing these materials into HPM sub-systems, such as NLTLs, requires characterizing this nonlinear behavior at microwave frequencies.

This study evaluates the nonlinear permeability of single and dual inclusion coaxial composites between 1-4 GHz to better understand their electromagnetic behavior and potential application for flexible HPM and NLTL systems. Section 3.2 summarizes the experimental materials and methods. Section 3.3 reports the measurements of permeability as a function of current for composites containing NZF inclusions or a combination of NZF and BST inclusions. We make concluding remarks in Section 3.4. This Chapter has been submitted to *IEEE Transactions on Magnetics* for consideration for publication.

3.2 Methods

We manufactured single inclusion composites containing various volume fractions of NZF or various volume fractions of NZF and BST. Table I summarizes the volume fractions used in these composites. Four samples of each volume fraction were fabricated to quantify statistical

variations in permeability measurements and to evaluate the reproducibility of the manufacturing procedure.

All composites used a two-part silicone base (Sylgard 184) as their host. The composites were manufactured with length $l \geq \lambda/4$, where λ is the wavelength, based on the lowest measured frequency with an inner diameter of 3 mm and an outer diameter of 7 mm. Scanning Electron Microscopy(SEM) revealed that the NZF inclusions mostly had aspect ratios typically less than unity while the BST inclusions were generally spherical. The manufacturers of the NZF (Powder Processing & Technology FP350) and BST (TPL Inc. HBS-8000) powders reported average inclusion sizes of 17 μm and 600-800 nm, respectively although SEM suggests a lower average inclusion size for the NZF inclusions. X-ray diffraction (XRD) performed on both the NZF and BST powder showed that the composition agreed well with the literature/commercial compositions of $Ni_{0.5}Zn_{0.5}Fe_2O_4$ and $Ba_{0.45}Sr_{0.55}TiO_3$ [29].

Table 1 Volume fractions of NZF and BST used in single and dual inclusion composites.

Single Inclusion NZF (%)	**Dual Inclusion (BST/NZF) (%)**	
5	5	5
10	5	10
15	10	5
20	10	10
25	10	15
/	15	10

The composites were manufactured by first measuring the mass of the PDMS and then calculating the mass of the powder needed to reach a desired volume fraction. The mixture was then centrifuged (Thinky Mixer AR-100) at 400 RPM. Composites containing BST were sonicated (Crest Ultrasonics CP200HT) for 4 hours to prevent conglomerations. We added the necessary

amount of curing agent, $1/10^{th}$ the mass of PDMS, and stirred the mixture by hand for 5 minutes. Both single and dual inclusion composites were then outgassed (Medline Scientific Jeio Tech 665L Vacuum Oven OV-12) for 5 minutes at 0.1 MPa before placing it into a mold. The molds were then outgassed for 5 minutes to ensure no air bubbles formed during the filling process. The samples were then placed into an oven (Blue M LO-136E) at 100 ºC for 2 hours to cure.

We next designed and constructed a multilayered DC solenoid. The solenoid frame was approximately 120 mm long; the solenoid was wrapped in 1200 turns of 14 Gauge AWG magnet wire 1.71 mm in diameter (with insulation) using a coil winding machine. The inner diameter of the solenoid frame was 1 in to fit a coaxial airline (Keysight Type-N 50 Ω Verification Kit) inside. The solenoid was wired to a current supply (Acopian Model #: Y050LX2B2880-DIO1) with a maximum output current of 28 A at 50 V. A digital interface communicated with the power supply by a computer to control the current and voltage ramp rate. Two fans were placed on each side of the coil to minimize the temperature increase, especially at higher currents. Internal temperatures were measured at three locations inside the solenoid frame using a digital infrared thermometer

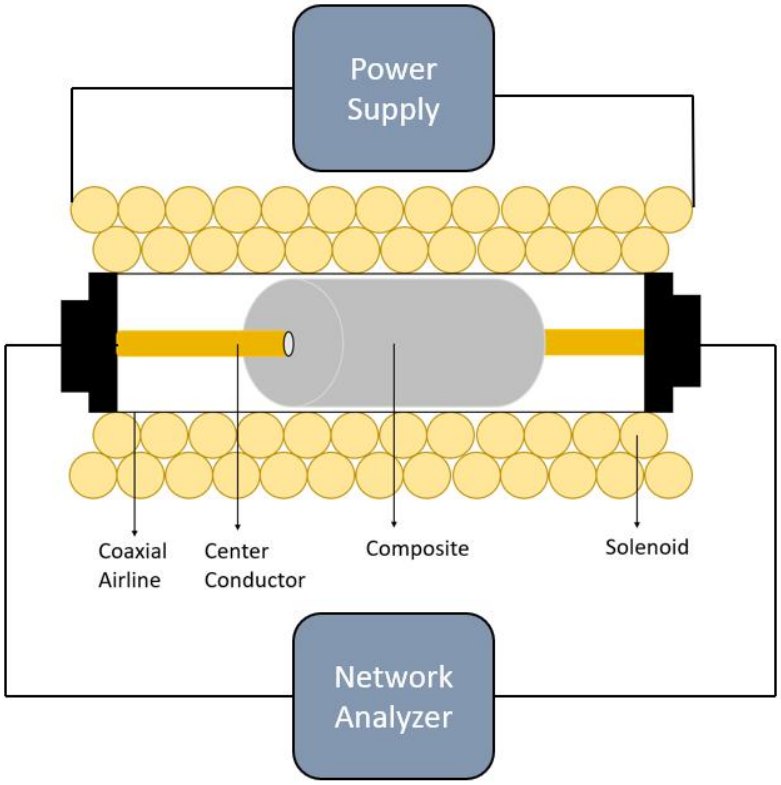

Figure 5 Experimental setup for measuring the nonlinear permeability of the composites. The composite was placed on the center conductor of the coaxial airline, which was placed inside a solenoid. After energizing the solenoid, we measured the S-parameters and imported them into commercial software to extract the permeability.

before and after each measurement to assess the uniformity and severity of the heating. A Gauss meter and axial probe (F.W. Bell 5186-110120) were used to measure the magnetic field to ensure field uniformity and strength inside the solenoid. figure 5 shows the experimental setup.

We accounted for losses associated with the coaxial airline by performing a full two-port calibration using a Keysight 85054D Calibration Kit. This calibration type achieves the most accurate measurement by accounting for the intrinsic systematic error associated with the network analyzer and coaxial airline. Samples were then inserted on the center conductor of the coaxial airline and their lengths measured using digital calipers. To mitigate the downtime between

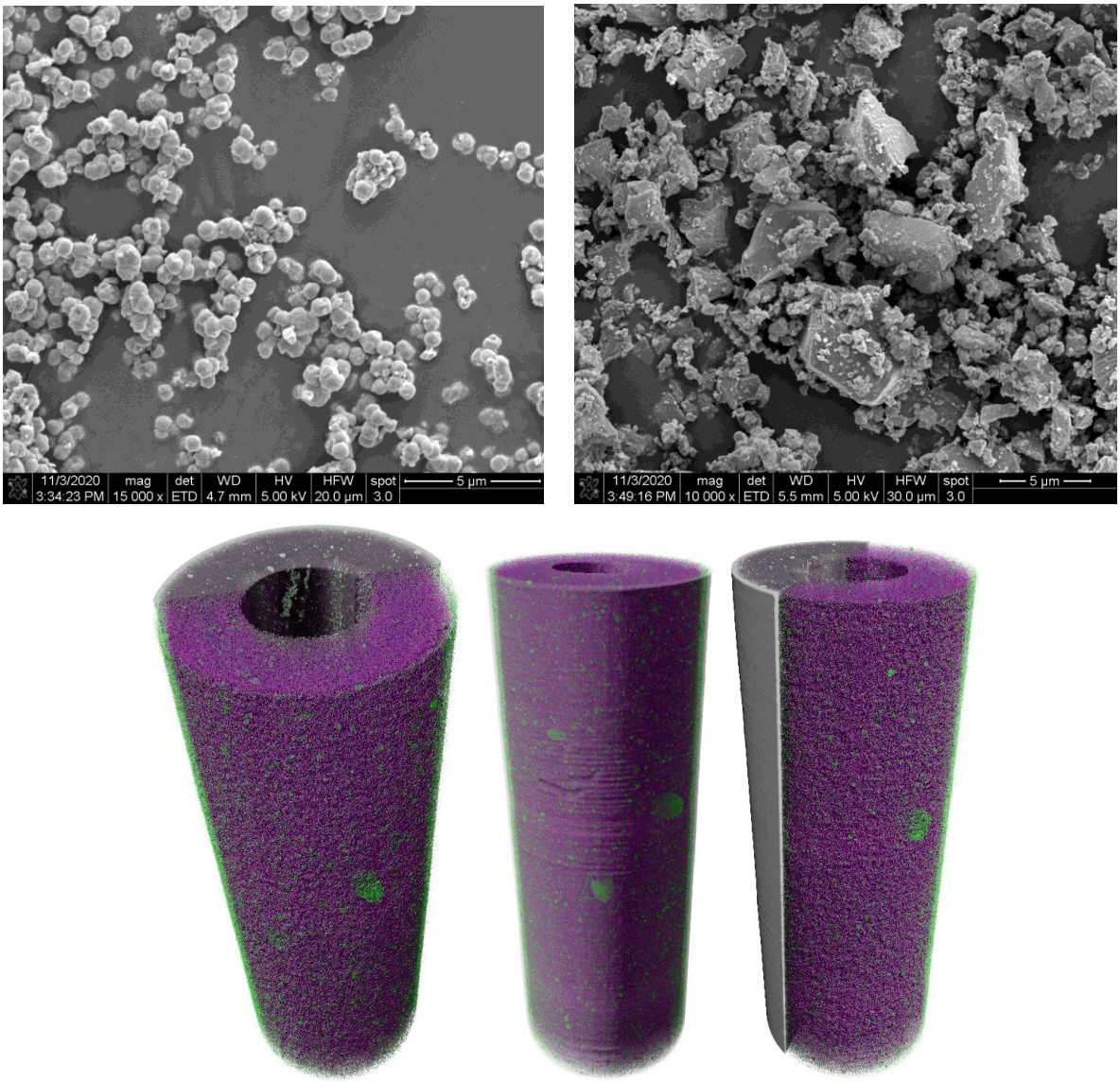

Figure 6 (Top) Scanning Electron Microscopy Images of BST(Left) and NZF(Right). (Bottom) 3D X-ray Microscopy images of a 15% BST (Purple) and 10% NZF (Green) composite used to assess the uniformity of the mixture.

measurements, we determined the interior temperature at which the solenoid naturally settled with successive 5, 10, 15, and 20 A measurements under active cooling. With the solenoid at room temperature (21 ºC), concurrent measurements at the above currents showed that the interior temperature of the solenoid increased by nearly 9 ºC. When allowed to warm to 30 ºC, the same current measurements yielded a maximum temperature transient of approximately 3 ºC. Thus, we allowed the solenoid's interior to warm to 30 ºC to better control and monitor the solenoid's temperature. Temperature transients inside the coil varied for each measurement since increasing

the current increased the heat produced. Fans actively cooled the coil's interior to 30 ºC before proceeding to the next measurement.

Using a network analyzer (Keysight FieldFox Handheld Microwave Analyzer N9913A), we measured the S-parameters of the coaxial airline from 1-4 GHz at solenoid currents of 0, 5, 10, 15, and 20 A (in that order). The S-parameters were then imported into commercial software (Keysight Material Measurement Suite Software Transmission Line and Free Space method) to calculate the permeability using the Polynomial Fit Reflection/Transmission Mu and Epsilon model, which is an iterative technique to fit material properties to a polynomial that is highly accurate for magnetic samples. The average number of scans per measurement was set to three; the number of points per scan was set to 601; the power was set to -15 dBm; and the intermediate frequency bandwidth (IFBW) was set to 1 kHz. The IFBW and average number of scan parameters are directly related to the overall speed of the measurement. After some trial and error, these settings were chosen to minimize the solenoid's operational time without compromising measurement accuracy.

To determine the statistical significance of the variation of permeability with volume fraction for a given field strength, we wrote a MATLAB script to perform a one-way analysis of variance (ANOVA). The output of the ANOVA test was then used to perform a multiple comparison test to generate a *p*-value that represents the likelihood of the observed value occurring due to chance. The standard used to determine statistical significance was $\alpha = 0.05$; therefore, $p < 0.05$ indicates statistical significance.

3.3 Results

3.3.1 Single Inclusion Results

The permeability and magnetic loss tangents of both single and dual inclusion composites are strongly coupled to the frequency and bias field strength [30]. The measured real composite permeability μ_{comp} decreased with increasing frequency; however, this behavior only became statistically significant at higher volume loadings of NZF. Figure 7 demonstrates this dependence

of μ_{comp} for 25% NZF composites at 1, 2, 3, and 4 GHz in the presence of applied magnetic fields of 0, 45.49 ± 2.06, 92.09 ± 4.06, 137.58 ± 9.07, 171.18 ± 5.07 kA/m.

At lower magnetic field strength $H \lesssim 100\ \mathrm{kA/m}$, μ_{comp} decreased with increasing frequency; for $H \gtrsim 100\ \mathrm{kA/m}$, μ_{comp} was insensitive to frequency. Also interesting, at 3 and 4 GHz, μ_{comp} increased with increasing H for $H \lesssim 100\ \mathrm{kA/m}$ but decreased with increasing H for $H \gtrsim 100\ \mathrm{kA/m}$. This frequency and magnetic field strength dependence of μ_{comp} have implications on NLTL design. NLTLs operating at these frequencies with a sufficiently high volume fraction of NZF can leverage the observed profile by biasing the composite at the appropriate H. In addition to aiding in coherent precession of the magnetic moments, this also maximizes the difference between μ at the crest of the pulse and the base of the pulse front, minimizing the rise time. Moreover, this capability of manipulating H for controlling phase velocity is promising for incorporating NLTLs into phased array systems to delay pulses using different field strengths [7].

To assess the impact of H on the composite, we considered the statistical significance of the observed changes at each frequency. An ANOVA test revealed that at 1 and 2 GHz, the changes observed for $H \lesssim 100\ \mathrm{kA/m}$ were never statistically significant; however, $H \gtrsim 100\ \mathrm{kA/m}$ induced statistically significant changes. At 3 and 4 GHz, the only insignificant changes occurred when comparing 45.49 ± 2.06 kA/m to 137.58 ± 9.07 kA/m and 0 to 171.18 ± 5.07 kA/m. Given the observed profile at these frequencies, this insignificance intuitively make sense.

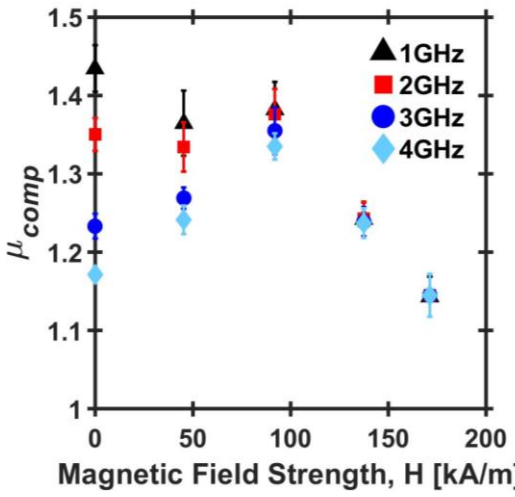

Figure 7 Real component of the relative permeability μ_{comp} of a composite consisting of 25% NZF inclusions in PDMS as a function of bias magnetic field strength at 1, 2, 3, and 4 GHz. The values reported are the mean of four measurements with error bars determined using standard deviation.

Assessing the impact of volume fraction on μ_{comp} is necessary to understand the potential implementation of dielectric and magnetic property manipulation for HPM system flexibility. Figure 8 shows μ_{comp} as a function of H for various volume fractions of NZF at 1, 2, 3, and 4 GHz. In general, μ_{comp} increases with increasing volume fraction, but this effect is significantly dampened at higher frequencies. Of similar interest is the nonlinearity of the permeability for each respective volume fraction. Significant changes in the permeability with respect to the magnetic field only occur when the NZF volume loadings $\geq 15\%$. Figure 8 also demonstrates the feasibility of using NZF volume loading to tune μ_{comp}, which could suggest the potential to tune NLTL impedance for matching to either a pulsed power driver or output. Figs. 7 and 8 also show the ability to control the permeability by using an external biased field to provide the operator greater control over the parameters of the RF pulse from the NLTL, such as rise time.

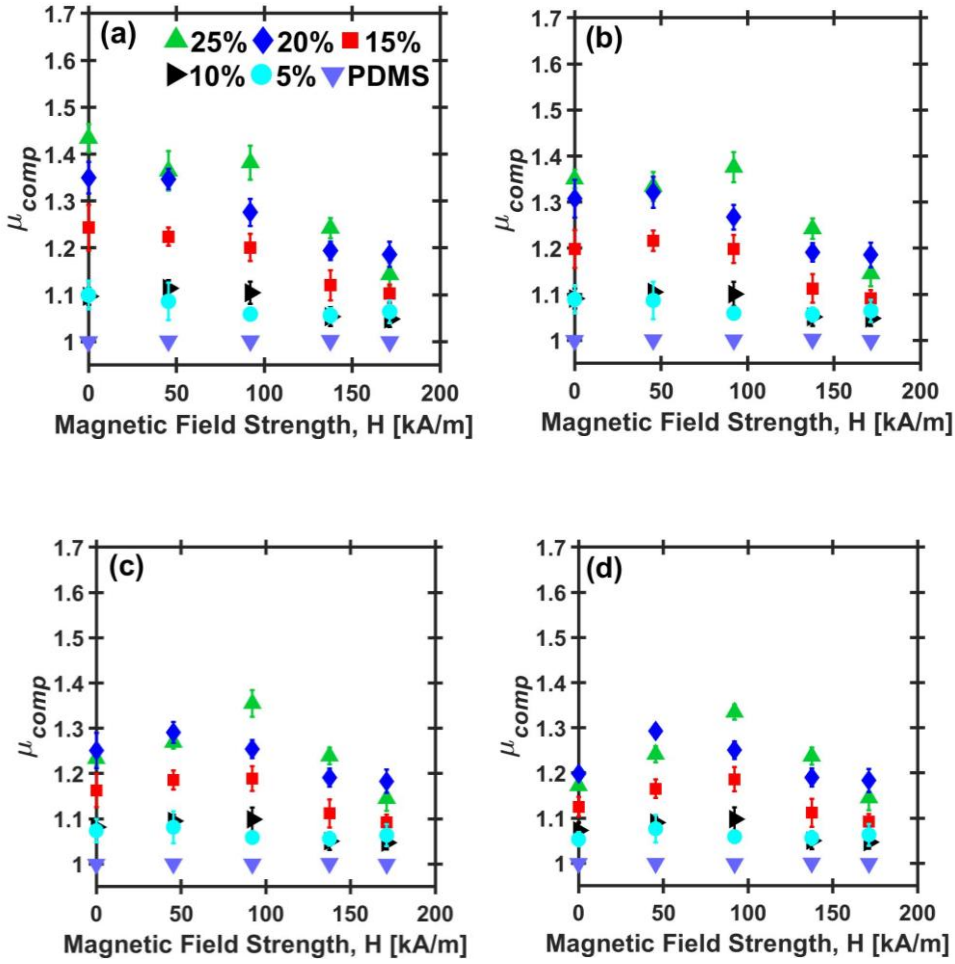

Figure 8 Variation in the real component of the relative permeability μ_{comp} of a composite with 0% (just PDMS), 5%, 10%, 15%, 20%, and 25% volume loadings of NZF inclusions in PDMS as a function of bias magnetic field strength at (a) 1 GHz and (b) 2 GHz (c) 3 GHz (d) 4GHz. The values reported are the mean of four measurements with error bars determined using standard deviation.

Table 2 summarizes the results of an analysis of variance (ANOVA) to assess the statistical significance of the differences and changes induced in μ_{comp} by altering the volume fraction. At all frequencies, the data for 10% NZF compared to the 5% NZF was never statistically significant. The difference between 25% NZF and 20% NZF was only significant at $H = 92.09 \pm 4.06$ kA/m. Changing volume fraction by more than 10% caused statistically significant differences in μ_{comp} for most field strengths and volume loading changes. The reduced statistical significance at higher field strengths is expected as we approach the saturation permeability. These results suggest that inclusion loading should be modified by at least 10% to induce noticeable changes in μ_{comp}.

Table 2 Statistical significance in μcomp for changes in volume loading

Field Strength (kA/m)	*f* (GHz)	25 to 20	25 to 15	25 to 10	25 to 5	20 to 15	20 to 10	20 to 5	15 to 10	15 to 5	10 to 5
0		0.05	**< 0.01**	**< 0.01**	**< 0.01**	**0.01**	**< 0.01**	**< 0.01**	**< 0.01**	**< 0.01**	1.00
45 ± 2.06		0.95	**< 0.01**	**< 0.01**	**< 0.01**	**< 0.01**	**< 0.01**	**< 0.01**	**< 0.01**	**< 0.01**	0.78
92 ± 4.06	1	**< 0.0**1	**< 0.01**	**< 0.01**	**< 0.01**	**0.03**	**< 0.01**	**< 0.01**	**< 0.01**	**< 0.01**	0.29
137 ± 9.07		0.14	**< 0.01**	**< 0.01**	**< 0.01**	0.09	**< 0.01**	**< 0.01**	**0.04**	0.05	1.00
171 ± 5.07		0.12	0.77	**< 0.01**	**0.01**	**0.01**	**< 0.01**	**< 0.01**	**0.02**	0.08	0.93
0		0.51	**< 0.01**	**< 0.01**	**< 0.01**	**0.01**	**< 0.01**	**< 0.01**	0.01	0.01	1.00
45 ± 2.06		0.98	**< 0.01**	**< 0.01**	**< 0.01**	**< 0.01**	**< 0.01**	**< 0.01**	**< 0.01**	**< 0.01**	0.94
92 ± 4.06	2	**< 0.01**	**< 0.01**	**< 0.01**	**< 0.01**	**0.04**	**< 0.01**	**< 0.01**	**< 0.01**	**< 0.01**	0.36
137 ± 9.07		0.12	**< 0.01**	**< 0.01**	**< 0.01**	**0.04**	**< 0.01**	**< 0.01**	0.07	0.11	1.00
171 ± 5.07		0.20	0.50	**< 0.01**	**0.01**	0.01	**< 0.01**	**< 0.01**	**0.04**	0.16	0.92
0		0.93	0.06	**< 0.01**	**< 0.01**	**0.01**	**< 0.01**	**< 0.01**	**0.02**	**0.01**	1.00
45 ± 2.06		0.98	**0.02**	**< 0.01**	**< 0.01**	**0.01**	**< 0.01**	**< 0.01**	**0.01**	**< 0.01**	0.97
92 ± 4.06	3	**< 0.01**	**< 0.01**	**< 0.01**	**< 0.01**	**0.03**	**< 0.01**	**< 0.01**	**< 0.01**	**< 0.01**	0.30
137 ± 9.07		0.12	**< 0.01**	**< 0.01**	**< 0.01**	0.05	**< 0.01**	**< 0.01**	0.06	0.09	1.00
171 ± 5.07		0.19	0.48	**< 0.01**	**0.01**	**0.01**	**< 0.01**	**< 0.01**	**0.03**	0.16	0.91
0		0.28	**0.02**	**< 0.01**	**< 0.01**	**< 0.01**	**< 0.01**	**< 0.01**	**0.01**	**< 0.01**	0.54
45 ± 2.06		0.77	**0.03**	**< 0.01**	**< 0.01**	**< 0.01**	**< 0.01**	**< 0.01**	**0.03**	**0.01**	0.97
92 ± 4.06	4	**< 0.01**	**< 0.01**	**< 0.01**	**< 0.01**	**0.02**	**< 0.01**	**< 0.01**	**< 0.01**	**< 0.01**	0.22
137 ± 9.07		0.14	**< 0.01**	**< 0.01**	**< 0.01**	**0.04**	**< 0.01**	**< 0.01**	0.05	0.09	1.00
171 ± 5.07		0.20	0.48	**< 0.01**	**0.01**	**0.01**	**< 0.01**	**< 0.01**	**0.03**	0.15	0.92

It is also critical to consider a material's magnetic losses when considering implementation into an NLTL system, specifically the dependence of the magnetic loss tangent on frequency and bias field strength. Figure 9 shows the magnetic loss tangent $\tan\delta$, given by the ratio of the imaginary permeability to the real permeability, for composites comprised of either 5% NZF or 25% NZF from 1-4 GHz as a function of *H*. As expected, the magnetic losses are heavily influenced by the volume fraction of NZF and frequency. Interestingly, the magnetic losses of the 25% NZF composite are strongly coupled to the external field strength, indicating the importance of adding more nonlinear inclusions into the composite. The results suggest that applying stronger external magnetic field strengths of 137.58±9.07 kA/m and 171±5.07 kA/m may suppress

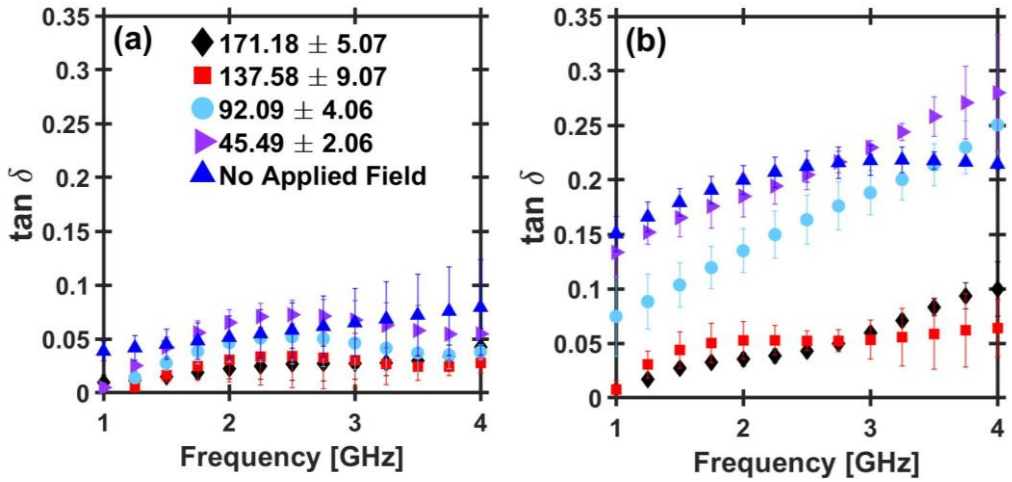

Figure 9 Magnetic loss tangent tan δ of (a) 5% NZF and (b) 25% NZF composites from 1-4 GHz for various external magnetic biasing field. Stronger magnetic biasing fields strongly suppresses the magnetic losses for the 25% NZF samples, while increasing the magnetic biasing field has a less noticeable effect on tan δ for the 5% NZF samples.

magnetic losses compared to no/low magnetic field strength. Equally important is that the magnetic loss tangents tend to be fairly small, which is necessary to achieve microwave oscillations [4].

Figure 10 presents the results of the ANOVA test performed to assess the statistical significance of the data in Figure 9. For 5% NZF, changes in the magnetic bias were generally only statistically significant at the lowest frequency when comparing the higher applied magnetic bias to no bias (e.g. 171 kA/m compared to 0 kA/m at 1 GHz). The changes observed for the 25% NZF data exhibit statistical significance across the entire frequency range for most magnetic field biases. This suggests that *H* plays a role in suppressing the magnetic losses at 25% NZF. Therefore, when designing an NLTL system utilizing ferrimagnetic material, external magnetic fields at higher volume loadings may minimize (or at least mitigate) magnetic losses, which is advantageous for maximizing the efficiency of the system. These results also demonstrate the importance of using a pulse of sufficient current to maximize the magnetic field inside the NLTL to reduce the magnetic losses.

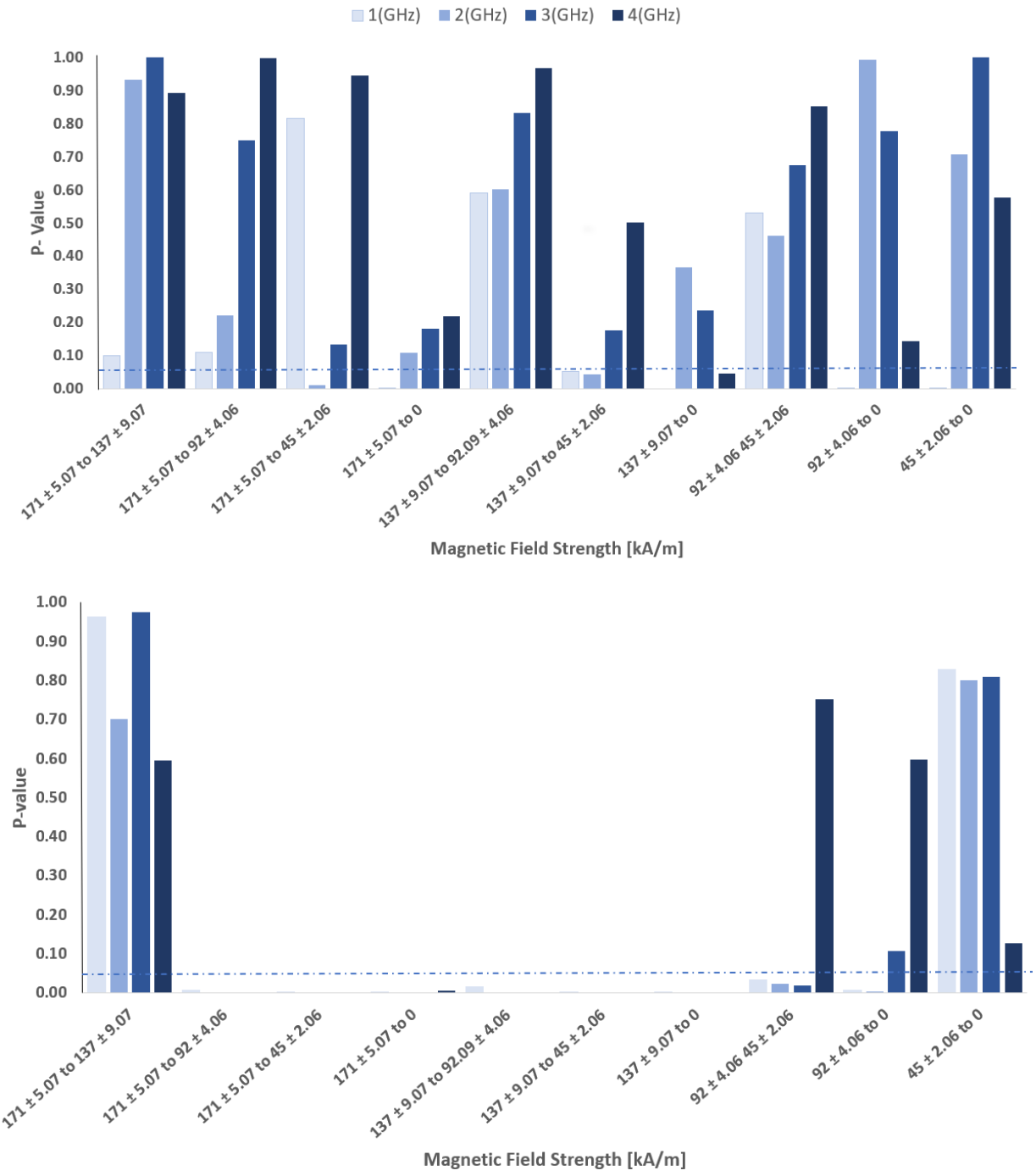

Figure 10 Results of the ANOVA and multiple comparison test on the magnetic loss tangent tanδ from Figure 5 for the 5% NZF (top) and 25% NZF (bottom) volume loadings where $p < 0.05$ indicates statistical significance. High statistical significance was achieved for th the 25% NZF magnetic losses which suggests the higher magnetic fields aid in the suppression of the magnetic losses. The statistical significance achieved for 5% NZF was typically achieved at the lowest frequency studied (1 GHz) and when comparing strong to weak magnetic fields (e.g. 171 kA/m to 0).

3.3.2 Dual Inclusion Composites

Dual inclusion composites containing various volume fractions of BST and NZF were manufactured and subjected to the same test methods as the single inclusion. Figure 11 shows that adding BST inclusions to a composite containing 10% NZF and PDMS will not influence μ_{comp}. This is advantageous because, while not measured here, adding BST inclusions increase the composite's permittivity, which should theoretically reduce the risk of breakdown between the center and outer conductors, while still permitting the use of *H* for biasing the NZF. Moreover, since BST exhibits

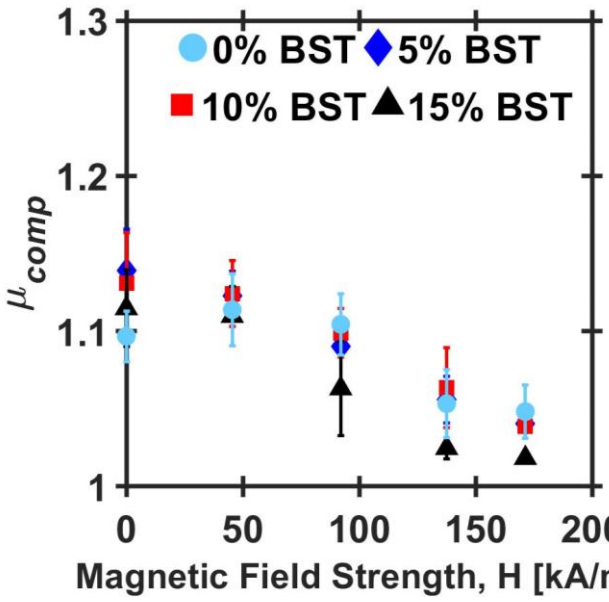

Figure 11 Relative permeability μ_{comp} of a composite containing 10% NZF and 0%, 5% , 10%, and 15% BST in PDMS as a function of bias magnetic field strength at 1 GHz. The permeability is not affected by the addition of BST. The values reported are the mean of four measurments with error bars determined using standard deviation.

nonlinear permittivity with electric field, combining BST and NZF may permit simultaneously achieving nonlinearity in both permittivity and permeability to form an electromagnetic shockwave.

The ANOVA test performed on the data from figure 11 and summarized in Table 3 confirms that adding BST to a composite with NZF generally does not change μ_{comp} significantly. It required the highest BST volume loading (15%) and highest magnetic field strength (171 kA/m)

considered here to cause a statistically significant change to μ_{comp} compared to the 10% NZF sample.

Table 3 Statistical significance of adding BST on μ_{comp} of a 10% NZF sample.

Field Strength (kA/m)	**171 ± 5.07**	**137 ± 9.07**	**92 ± 4.06**	**45 ± 2.06**
5% to 10%	1.00	0.95	0.97	1.00
5% to 15%	0.05	0.21	0.53	0.82
5% to 0%	0.70	1.00	0.89	0.93
10% to 15%	0.06	0.09	0.31	0.78
10% to 0%	0.58	0.90	0.99	0.90
15% to 0%	**0.01**	0.27	0.21	0.99

Figure 12 shows the effect of BST volume loading on magnetic loss tangents for a 10% NZF composite. In general, the changes observed were not statistically significant for much of the frequency range; however, the difference between the 10% NZF/15% BST loading and the 10% NZF composite was statistically significant. This is surprising since BST is inherently nonmagnetic and warrants further investigation into characterizing the potential mechanisms by which BST may suppress magnetic losses. One potential reason could be that adding a sufficient volume loading of BST, which is strongly insulative, disrupts the connectivity of the NZF inclusions, subsequently reducing the strength of the magnetic behavior. Further supporting this argument is the size of the BST particles (~600-800 nm) allows it to wedge between the much larger NZF. Table 4 reports the *p*-values from the ANOVA.

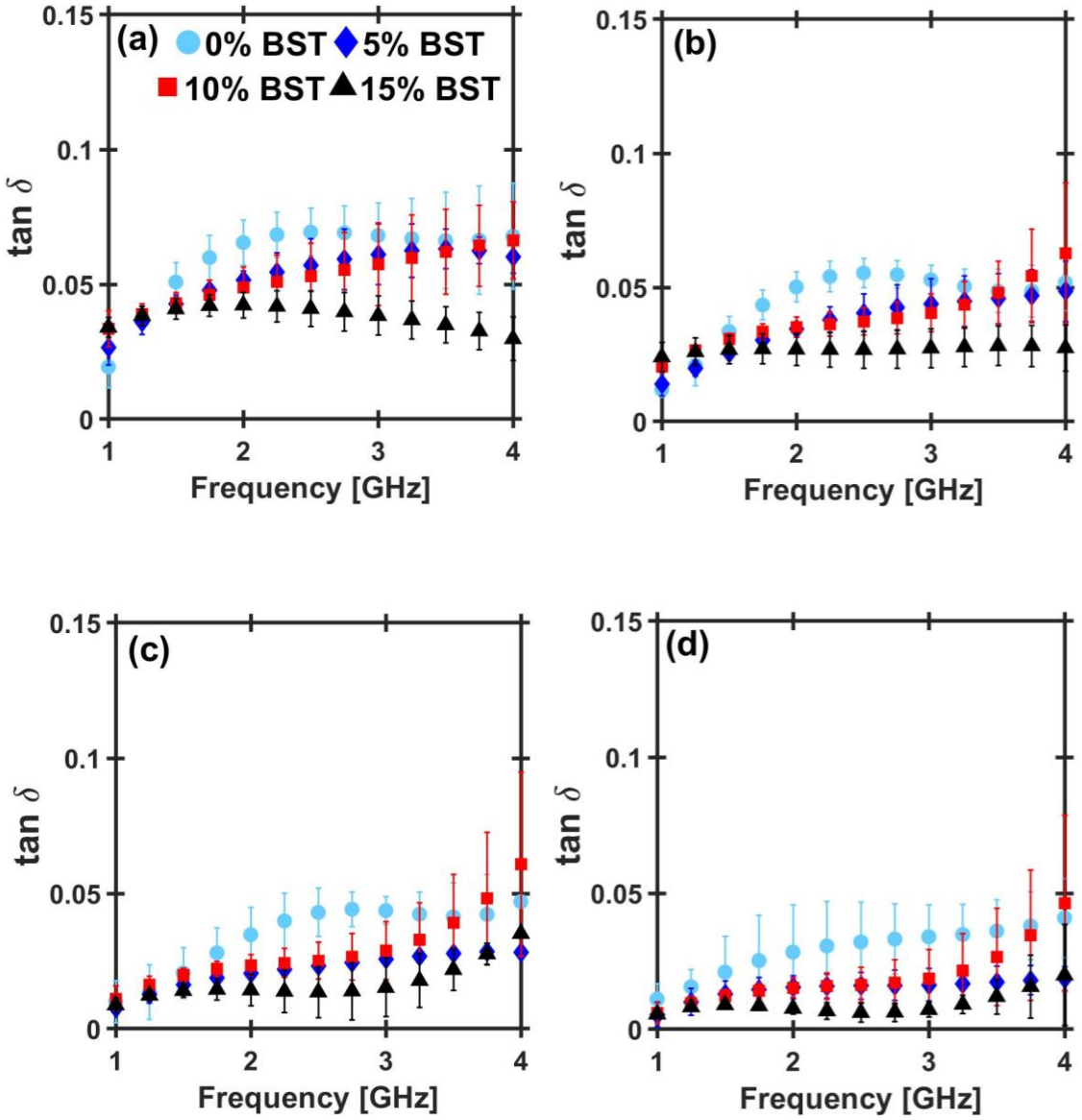

Figure 12 Magnetic losses for a 10% NZF composite with varying volume fractions of BST at (a) 45 ± 2.06 (b) 92 ± 4.06 (c) 137 ± 9.07 (d) 171 ± 5.07 kA/m from 1-4 GHz.

Table 4 Statistical significiance of adding BST on the magentic loss tangents of a 10% NZF composite.

Frequency (GHz)	**Field Strength**	**5% to 0%**	**10% to 0%**	**15% to 0%**
1	45 ± 2.06	0.527	0.056	**0.044**
	92 ± 4.06	0.814	**0.013**	**0.010**
	137 ± 9.07	0.940	0.991	0.991
	171 ± 5.07	0.360	0.391	0.389
2	45 ± 2.06	0.076	**0.021**	**0.003**
	92 ± 4.06	**0.003**	**0.003**	**0.000**
	137 ± 9.07	0.064	0.121	**0.008**
	171 ± 5.07	0.389	0.315	0.095
3	45 ± 2.06	0.875	0.626	**0.030**
	92 ± 4.06	0.416	0.156	**0.004**
	137 ± 9.07	**0.048**	0.077	**0.003**
	171 ± 5.07	0.118	0.146	**0.015**
4	45 ± 2.06	0.867	0.998	**0.009**
	92 ± 4.06	0.995	0.838	0.303
	137 ± 9.07	0.603	0.762	0.854
	171 ± 5.07	0.539	0.984	0.585

In general, adding 5 and 10% BST does not result in a statistically significant change in loss tangent ($p > 0.05$). Most statistically significant changes ($p < 0.05$) occur at 2 and 3 GHz when comparing 15% BST to 0% BST. All statistically significant changes ($p < 0.05$) are in bold.

3.4 Concluding Remarks

This chapter reports the nonlinear permeability of composites containing various volume loadings of NZF or combinations of NZF and BST between 1 and 4 GHz. The permeability of the NZF composites depended strongly on frequency, external magnetic field strength, and volume loading. Statistically significant changes in the composite's permeability with respect to the magnetic field strength required NZF volume loadings of at least 15% NZF. Statistically significant changes in the permeability with respect to volume loading required at least a 10%

change in NZF volume loading at most magnetic field strengths, although composites with 5% changes in NZF volume loading were, on average, statistically significant at low magnetic field strengths but became insignificant at higher magnetic field strengths. When investigating the effect of frequency on the composites, the observed profile suggested that NLTLs at 3 and 4 GHz could leverage biasing the line at the appropriate H to maximize the lines pulse sharpening and microwave generation capabilities. This phenomenon would occur since the permeability seen by the crest of the pulse and foot of the pulse would be maximized. For dual inclusion composites, adding BST did not induce statistically significant changes in the permeability except when comparing a 15% BST/10% NZF to a 0% BST/10% NZF sample at 171 kA/m. The magnetic loss tangents for single and dual inclusion composites depended strongly on the magnetic field strength, generally exhibiting lower loss tangents at higher external field values. For dual inclusion composites, adding a sufficient volume loading of BST to an NZF composite suppressed magnetic losses. Future studies may explore whether this behavior arises due to the total volume loading of all (NZF and BST) inclusions or BST disrupting the NZF network, reducing the magnetic effects.

Long-term, characterizing the behavior of these composites will permit the construction of composite-based NLTLs with various nonlinear permittivity and permeability. This flexibility may permit tuning the output RF from the NLTL or match the NLTL to a given load based on adjusting volume loading of nonlinear dielectric or magnetic inclusions. Of particular importance, changing the composition of NZF can change its permeability, which can then alter composite permeability. The approach and results presented here provide a process for measuring and assessing the nonlinear permeability for such materials.

4. IMPEDANCE MATCHING AND ELECTRICALLY TAPERED LINES

Broadly speaking, most conventional HPM systems are comprised of three main components: a pulsed or prime power driver, an RF source, and an antenna/load. Within this grand scheme of the HPM system, it is paramount that all subcomponents be impedance matched to mitigate signal reflections and maximize power transfer [31],[32]. Failure to match each subcomponent can result in a large standing wave between the load and generator. This ultimately decreases the system's power handling capabilities since for a given amount of power transfer the field strength needed for dielectric breakdown is reached sooner [31]. Here, we briefly investigate the various ways in which subcomponents are commonly impedance matched and then propose our own method for impedance matching using the composite parameters from the previous chapter.

4.1 Stub Matching

One of the simplest ways to match a transmission line to a complex load is through stub matching. A stub match consists of shorted or open segments of transmission line, called stubs, attached in parallel or series with the main line. There are generally two primary design considerations when designing this matching network; the length of the stub l and the distance the stub is placed from the load d [31],[33]. Consider a voltage wave propagating from left to right, as shown in figure 13. When the wave reaches the junction between the stub and the main line, some of the wave propagates towards the load and some the wave propagates down the stub. When the wave reaches the end of the stub or the load, some of the wave is reflected. If both reflected waves are out of phase and equal in amplitude, then they will cancel. Therefore, when looking from the junction toward the load, one sees zero reflection, which is only possible when the impedance is matched. When the stub is placed in parallel with the load, it is more common to mathematically determine the necessary distance by working with admittances [31]. One places the stub a specific distance from the load to match the real part of the stub and the main line's admittance. The length of the stub is then chosen such that it has a complex input admittance exactly opposite of the line, resulting in a matched condition. The primary drawback of this technique from a system flexibility standpoint is changing the load requires moving the stub.

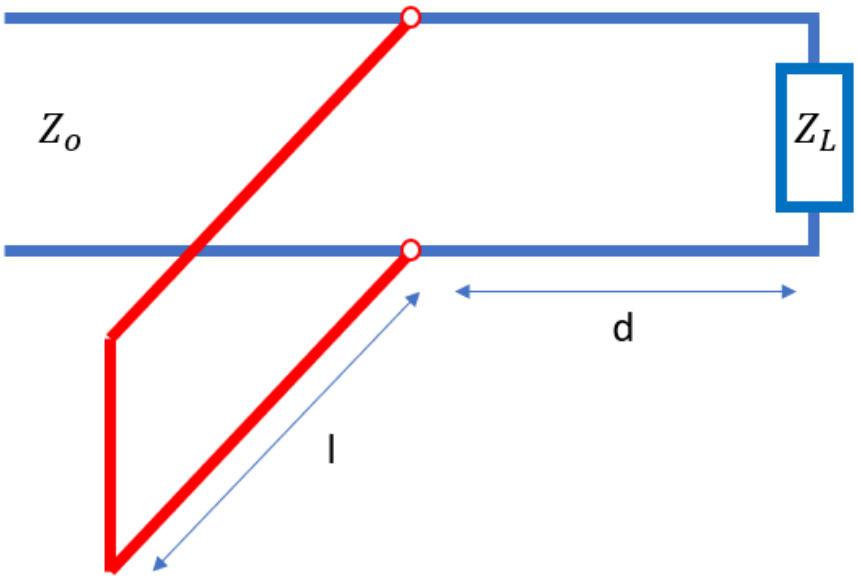

Figure 13 An example of a single stub matching circuit. The stub of length *l* is placed a distance from the load *d* such that the reflection waves have equal amplitude and opposite sign.

4.2 Quarter Wave Transformers

Quarter wave transformers are the basis for many matching networks primarily because they are simple to manufacture and implement. However, it is generally not until frequencies of hundreds of MHz to low GHZ that these matching networks become practical given the long wavelengths at lower frequencies [31],[34],[35]. Quarter wave transformers generally consist of intermediate sections of transmission line, a quarter wavelength of the center frequency long, with a characteristic impedance such that the load impedance is transformed into the same impedance as the line.

For a transmission line of characteristic impedance Z_1 attached to a simple single section quarter wave transformer with impedance Z_2 attached to a purely resistive load Z_l, the effective load impedance seen by the transmission line is given by [31]

$$Z_1 = Z_2 \frac{Z_l + jZ_2 \tan(\beta L)}{Z_2 + jZ_l \tan(\beta L)} \tag{8}$$

Noting that $\beta = 2\pi/\lambda$, we consider the case where the length of the line is chosen to be $L = \lambda/4$. we can factor out the tangent term on the numerator and denominator resulting in

$$Z_1 = Z_2 \frac{\tan\left(\frac{\pi}{2}\right)}{\tan(\frac{\pi}{2})} \frac{(\frac{Z_l}{\tan\left(\frac{\pi}{2}\right)} + jZ_2)}{(\frac{Z_2}{\tan\left(\frac{\pi}{2}\right)} + jZ_l)} = \frac{Z_2^2}{Z_l} \tag{9}$$

Therefore, since one wants the line impedance to equal the load impedance, we see that this condition is met if the impedance of the single quarter wave transformer,Z_2, is chosen to be $\sqrt{Z_1 Z_l}$. Single quarter wave transformers are great for impedance matching if matching over a narrow band is desirable; however, several quarter wave transformers are necessary to successfully match over a wide frequency band [31],[35]. Several studies have been done regarding the extension of quarter wave transformers to multi-section and *n*-section transformers [35] [36]. In general, the analysis of these transformers starts with developing an expression for the reflection coefficient so one can describe the systems pass band characteristics. In n-section transformers, the analysis lends

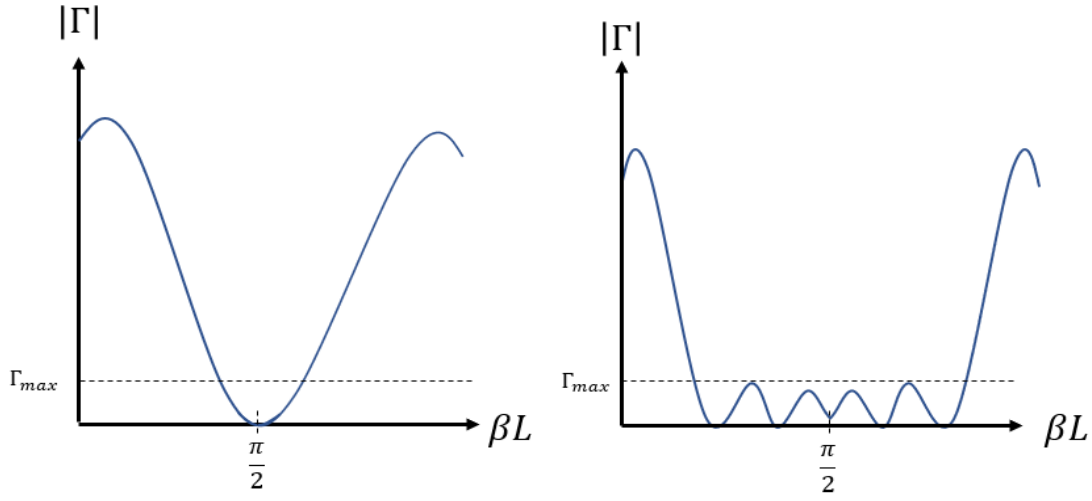

Figure 14 The reflection coefficient behavior of binomial and Chebyshev quarter wave transformers.

itself to the theory of small reflections which states that if the mismatch between sections is sufficiently small, only the first order reflections are important. This approximation led to the representation of the total reflection coefficient by a Fourier series. With these expressions developed, any desired reflection coefficient behavior over a given frequency could be achieved by choosing the appropriate coefficients and number of sections. This method is commonly referred to as the synthesis problem which refers to the designer choosing the coefficients in the Fourier series such that they give the desired pass band characteristics. This ultimately led to the development of binomial and Chebyshev transformers which are quarter wave transformers whose reflection coefficient behaviors are described by binomial and Chebyshev functions. They were designed to give the reflection coefficient which gave the maximally flat and equal ripple response over the passband respectively [31]. Figure 15 demonstrates how the reflection coefficient behaves for both these quarter wave transformer types where βL represents the electrical length. From the figure one sees that the binomial transformer has a passband characteristic that is maximally flat at a given frequency and, therefore, has a shorter bandwidth than the Chebyshev transformer, which maintains a reflection coefficient below the maximum of the passband ρ_m over a broader range of frequencies.

4.3 Non-Uniform Transmission Lines

Another method for matching impedances between subcomponents of a system is through non-uniform transmission lines. In contrast to the quarter-wave transformer, one can alternatively design a nonuniform transmission line whose impedance profile transitions smoothly rather than in discrete steps. Since, in practice, manufacturing a perfectly continuous tapered transmission line

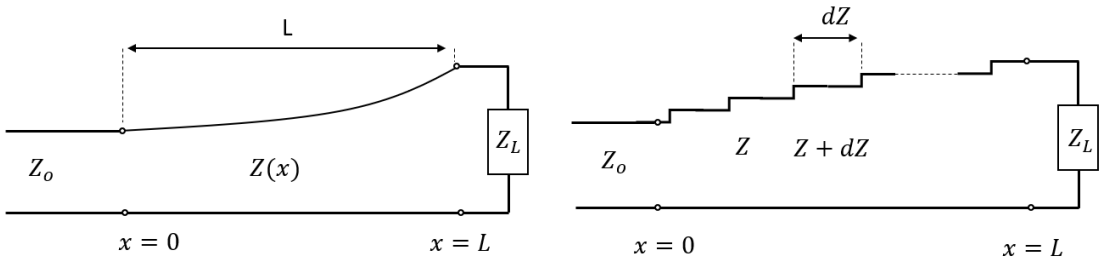

Figure 15 A non-uniform transmission line and its approximation by using discrete impedance steps.

is difficult and cumbersome, the theory typically lends itself to an approximation similar to that of the quarter wave transformer by considering the line as comprised of a discrete number of sections, as shown on the left in figure 15. The profile in figure 15 is achieved by geometrically altering the transmission line as a function of position. Changing the geometry allows the variation of the inductance and capacitance along the line to achieve the necessary impedance [31].

Most tapers generally lend themselves to three types of impedance profiles: exponential, triangular, and Klopfenstein, each with its respective advantages and disadvantages [37]-[40]. For example, the triangular taper has an overall smaller reflection coefficient in the passband compared to the exponential taper, while the exponential taper enters the pass band faster, meaning that the first minimum of the reflection coefficient occurs at a shorter length [31]. Klopfenstein tapers have similar passband characteristics in comparison to triangular tapers in that the magnitude of the reflection coefficient is significantly less than the exponential taper [51]. Although, Klopfenstein tapers are mathematically hard to work with making modeling and manufacturing very complicated [51]. Each style of taper has its respective place depending on the application. Where device miniaturization is preferred such as in microstrip systems, exponential tapers are often preferred by designers whereas triangular and Klopfenstein tapers are preferred for maximizing power transfer over a broader band of frequencies [51].[52]. The choice of taper is purely dependent on the desired pass band characteristics and typically a tradeoff between taper length and power transfer has to be made by the designer. As was the case with the multi-section transformer, understanding the behavior of the reflection coefficient for each profile is crucial for determining the total length of the taper and the maximum length of each section. Therefore, it is worth investigating how the reflection coefficient is generally determined for non-uniform lines.

Using figure 15 as a model, we note that each step change in impedance causes a differential reflection coefficient given by

$$d\rho = \frac{(Z + dZ) - Z}{(Z + dZ) + Z} = \frac{dZ}{2Z + dZ} \approx \frac{dZ}{2Z} = \frac{1}{2} d(\ln(Z)) = \frac{1}{2} \frac{d}{dx} (\ln(Z))\, dx. \tag{10}$$

The contribution to the input reflection coefficient is the product of $d\rho$ multiplied by a term representing the retardation introduced to the backward propagating wave since each reflection has to travel a different distance to reach the input [31], yielding

$$d\rho_i = \frac{d}{dx}\frac{(\ln(Z)\,dx)}{2}e^{-j2\beta x}, \tag{11}$$

where $\beta = 2\pi/\lambda$. Assuming that the sum of all the differential reflection coefficients is the total reflection coefficient, which is generally valid for $d\rho \leq 0.2$, gives the total reflection coefficient given as [31]

$$\Gamma_i = \int_0^L d\rho_i = \int_0^L e^{-j2\beta x} * \frac{d}{dx} * \frac{\ln(Z)\,dx}{2}. \tag{12}$$

The importance of (12) is that it allows us to determine the reflection coefficient for any continuous variation of *Z*, which is important for determining the necessary total length of the taper.

4.4 Electrically Tapered Lines

In chapter 3, it was demonstrated that by manipulating the volume loading of inclusions, one could effectively tune the electromagnetic properties of a composite. Leveraging this concept, we hypothesize that to bypass the challenges of manufacturing complex geometries and to provide greater system flexibility, one could rather electrically taper the transmission line. Such a line could consist of discrete sections of coax, each with a different volume loading of material, linked together to gradually adjust the line's impedance. Here, we develop this concept along with looking at previous works and combine this with effective medium theories (EMTs) to predict the necessary volume loadings of material for certain impedance profiles. This would allow one to match the output impedance of different pulsed power drivers and antennas thus enhancing the flexibility and rigidity of the system. To further elucidate the feasibility of this concept, we start by looking at past work which has implemented the concept of dielectric tapering.

The concept of dielectric tapering has most commonly found footing amongst the antenna community and the development of dielectric rod antennas. In tapered dielectric rod antennas, the

cross section of the rod decreases in the direction of propagation to allow the wave to gradually be transformed from a bound wave to one which exists in free space with minimal reflections occurring at the interface between the rod and the environment [41]. Studies have shown that single dielectric rod antennas can guide fundamental modes if the diameter of the rod is such that [42]

$$d < \frac{0.626\lambda_0}{\sqrt{\epsilon_o \epsilon_r}} \tag{13}$$

Resulting in significant bandwidth limitations. To overcome this hurdle, designers have utilized dielectric rods consisting of multiple concentric layers of dielectric whose permittivity increases with decreasing radius as the line is tapered [43]. Figure 16 depicts how this change in permittivity looks in practice.

Alternatively, dielectric tapers have also been used in transformation optics to control electromagnetic wave propagation [44]. For example, a continuously tapered permittivity field structure was 3D printed and tested over 7-13 GHz to match different size waveguides in Ref. [44]. Of particular interest here is the implementation of 3D printing in the manufacturing process to greatly reducing the complexity of taper manufacturing.

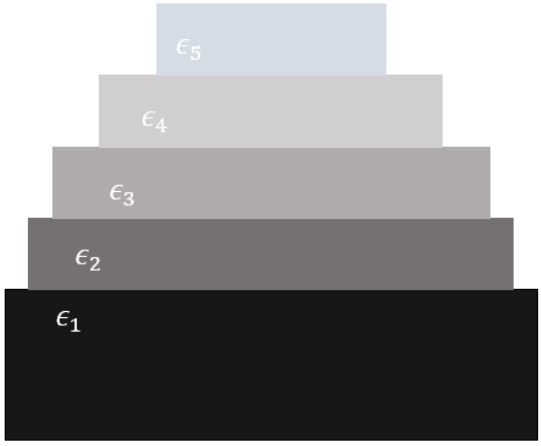

Figure 16 Example of how the permittivity profile of a dielectric rod antenna changes with decreasing diameter.

We note that the aforementioned tapers still require geometrical modification but lays the framework for the idea of tapering based on varying a material's electromagnetic properties. With

this in mind, we now investigate the feasibility of electrically tapered transmission lines with constant geometry for impedance matching as detailed in figure 17.

For a coaxial transmission lines with constant permittivity ϵ and permeability μ , the impedance is given by

$$Z = \sqrt{\frac{L}{C}} = \frac{\ln\left(\frac{b}{a}\right)}{2\pi}\sqrt{\frac{\mu}{\epsilon}}, \tag{14}$$

where b is the outer diameter and a is the inner diameter and $\mu = \mu_o\mu_r$ and $\epsilon = \epsilon_o\epsilon_r$. Note that μ and ϵ are typically considered as constants, although they may, in principle, vary with location along the line, as we shall discuss shortly. While the profile of the impedance taper selected by the designer is somewhat arbitrary, an exponential impedance profile gives the shortest line, which is advantageous for developing a compact system [31]. In coaxial lines, this is typically achieved by changing the ratio of the inner and outer diameters of the coaxial line as a function of position. The logarithmic dependence makes it natural to accomplish this by having b and a vary exponentially. Fixing b/a with $\mu(x)$ and $\epsilon(x)$ varying exponentially with position along the line by

$$\mu(x) = \mu\,(0)e^{\pm kx} \tag{15}$$

and

$$\epsilon(x) = \epsilon\,(0)e^{\pm kx} \tag{16}$$

yields an exponentially varying impedance profile, given by

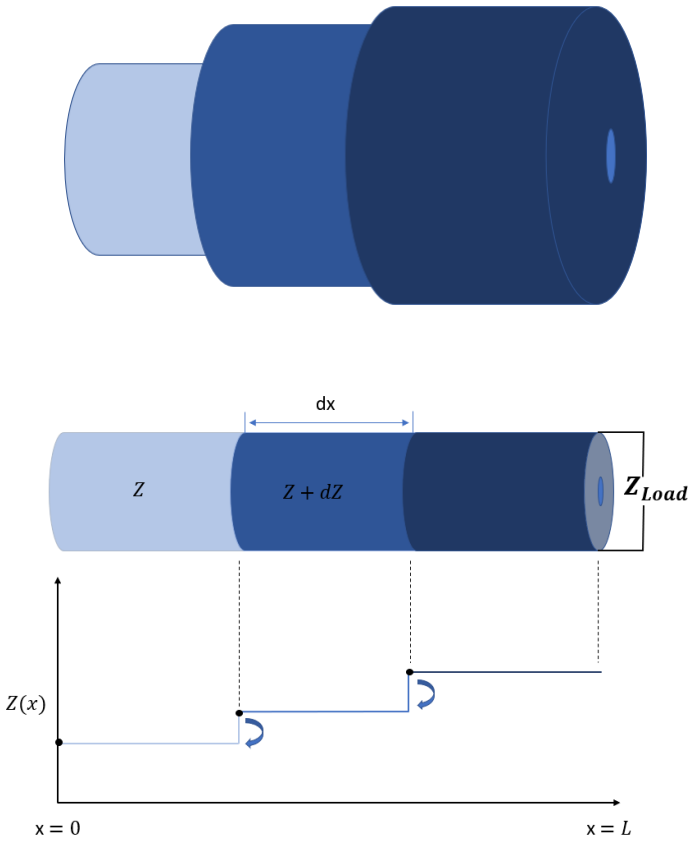

Figure 17 (Top) Traditional impedance taper achieved by geometrically changing the ratio of the inner and outer diameter of the coaxial line (Bottom) the proposed tapered line with fixed geometry but varying section impedance by adjusting inclusion volume loading.

$$Z(x) = \frac{\ln\left(\frac{b}{a}\right)}{2\pi}\sqrt{\frac{\mu(x)}{\epsilon(x)}} = \frac{\ln\left(\frac{b}{a}\right)}{2\pi}\sqrt{\frac{\mu(0)e^{\pm kx}}{\epsilon(0)e^{\pm kx}}} = \frac{\ln\left(\frac{b}{a}\right)}{2\pi}\sqrt{\frac{\mu(0)}{\epsilon(0)}}e^{\pm kx} = Z_i e^{\pm kx}, \qquad (17)$$

where $Z_i = \ln(b/a)\,(\mu(0)/\epsilon(0))^{1/2}/(2\pi)^{1/2}$ is the impedance at x = 0. Therefore, allowing the permeability and permittivity to vary exponentially with position as defined in (15) and (16) results in an exponential impedance. Plugging this impedance profile into the reflection coefficient equation (12) and noting that $\beta = 2\pi f\sqrt{\mu(x)\epsilon(x)}$ is independent of position if the permeability and permittivity vary as described in (15) and (16), we obtain

$$\Gamma_i = \frac{1}{2} e^{-2j\beta l} \ln\left(\frac{Z_l}{Zo}\right) \frac{\sin(\beta l)}{\beta l}. \tag{18}$$

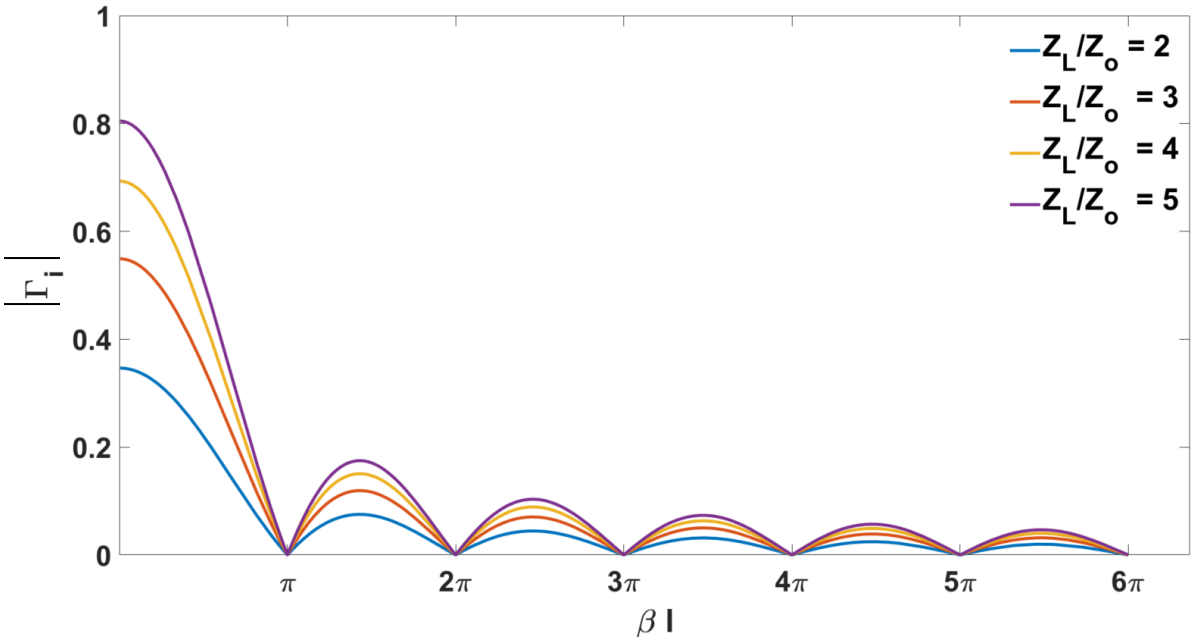

Figure 18 Input reflection coefficient for different taper ratios plotted as function of βL

We can plot the absolute value of (18) as a function of βl which is the electrical length, to work out how long the taper should be as was done with the quarter wave transformers. Figure 18 shows that the reflection coefficient is smallest when $\beta l = n\pi$. Since $\beta = 2\pi/\lambda$, this minimum corresponds to line lengths of multiples of half wavelengths. With the necessary total line length worked out, we can return to (10) and plot $d\rho$ as a function of dx and determine the maximum length of each section necessary to maintain a $d\rho \leq 0.2$ so that the theory of small reflections holds.

We can extend the above procedure to the nonlinear case, except that we also have to account for additional dependence of the permittivity and/or permeability on the voltage and/or current, respectively. Since NZF varies nonlinearly with permeability but not permittivity, and we seek a taper that varies exponentially with position, we define our material properties similar to Ref. [12] as

$$\epsilon(x) = \epsilon_{comp}(x) \tag{19}$$

$$\mu(x, I) = \mu_{comp}(x)(1 - b_1 I), \tag{20}$$

where b_1 is the nonlinearity factor for the current dependence. While other approximations for the voltage and current dependence give better fits for bulk ferrites [11],[10]; this approach is more mathematically tractable while agreeing reasonably well with our observed experimental composite behavior at 1 GHz, as shown in figure 19

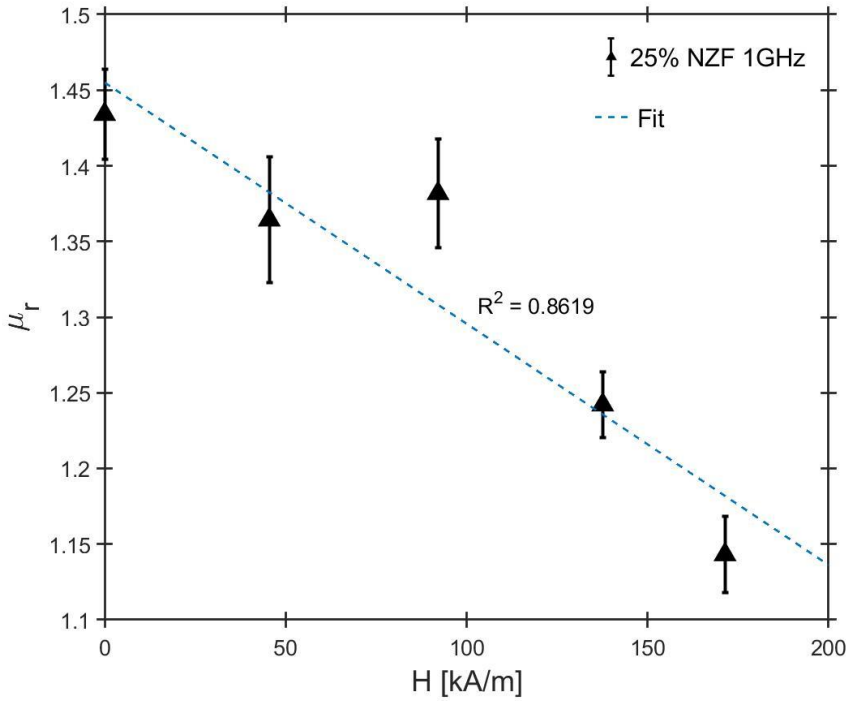

Figure 19 1 GHz data for a 25% NZF composite with a linear fit with R^2= 0.8619

At 2, 3 and 4 GHz, the model would most likely need to be adapted. The selection of $\mu_{comp}(x)$ and $\epsilon_{comp}(x)$ should be chosen to achieve the appropriate impedance profile. In the linear case, we allowed the permittivity and permeability to vary exponentially as a function of position. We can similarly modify (19) and (20) to obtain

$$\epsilon(x) = \epsilon_{comp} e^{\pm kx} \tag{21}$$

and

$$\mu(x, I) = \mu_{comp} e^{\pm kx}(1 - b_1 I), \tag{22}$$

where ϵ_{comp} and μ_{comp} are the permittivity and permeability, respectively, at x = 0. The impedance as a function of current and position in a coaxial line becomes

$$Z(x, I) = \frac{\ln\left(\frac{b}{a}\right)}{2\pi} \sqrt{\frac{\mu_{comp} e^{\pm kx}(1 - b_1 I)}{\epsilon_{comp} e^{\pm kx}}} = Z_i e^{\pm kx} \sqrt{1 - b_1 I} \tag{23}$$

Recall that in section 4.3, we developed a general method for approximating the reflection coefficient. To extend this method to the nonlinear case, we make the following observations. First, with no pulse propagating down the line, (23) reduces to the linear case as $I \rightarrow 0$. Second, when a current pulse propagates through each section of the line, (23) shows that the nonlinear impedance is simply the linear impedance multiplied by a number less than unity, making the impedance slightly lower than the baseline linear value. Assuming infinite rise and decay times, the impedance behaves as depicted in figure 20. Therefore, as a pulse of current propagates down a line, the nonlinear impedance Z_{NL}within the section with the pulse is less than the linear value Z_L, or $Z_{NL} < Z_L$. This means that the impedance the pulse front sees is actually the linear impedance, resulting in a small differential reflection coefficient given by

$$d\rho_{NL} = \frac{(Z_L - Z_{NL})}{(Z_L + Z_{NL})} e^{-j2\beta x}. \tag{24}$$

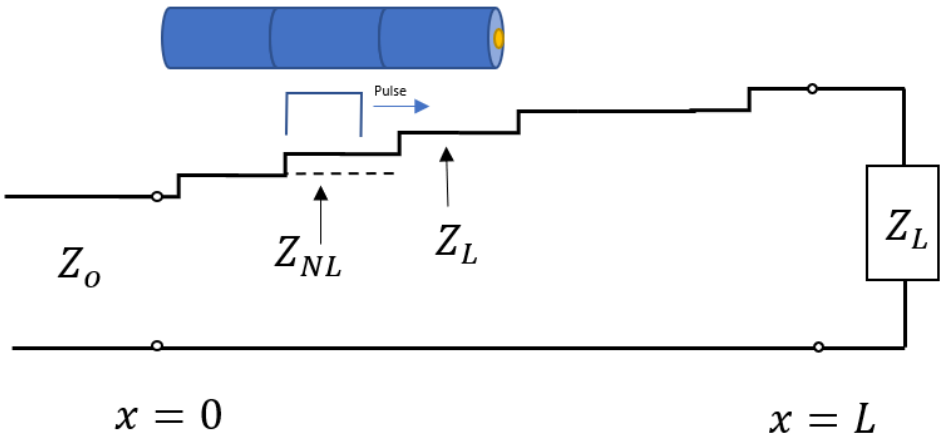

Figure 20 The approximation of a transmission lines impedance profile for linear and nonlinear lines.

For the exponential taper, the nonlinear and linear impedances are given by

$$Z_{NL} = Z_i e^{\pm kx}\sqrt{1 - b_1 I} \tag{25}$$

and

$$Z_L = Z_i e^{\pm kx}, \tag{26}$$

respectively. Substituting (25) and (26) into (24) yields

$$d\rho_{NL} = \frac{1 - \sqrt{(1 - b_1 I)}}{1 + \sqrt{(1 - b_1 I)}}. \tag{27}$$

As for the linear case, we assume that the total reflection coefficient is the sum of the first order reflections as the wave propagates, or

$$\Gamma_{i_{NL}} = \int_0^L d\rho_{NL} = \int_0^L e^{-j2\beta x} \frac{1-\sqrt{(1-b_1 I)}}{1+\sqrt{(1-b_1 I)}} dx \tag{28}$$

Without a constitutive relation for the current, we assume that the current within each section is constant, which only holds for sufficiently small ($\lambda/10$), lossless sections. Evaluating the integral in (28) yields

$$\Gamma_{i_{NL}} = \frac{e^{-i\beta L} \sin(\beta L)\,(-2 + b_1 I + 2\sqrt{1-b_1 I}\,)}{b_1 I \beta} \tag{29}$$

Similar to the linear case, (29) has a sinusoidal dependence with a minimum reflection coefficient when $\beta l = n\pi$ suggesting that the tapered section total length should still be an integer multiple of the half wavelength.

4.5 Implementing Effective Medium Theories

Over the last century, effective medium theories (EMTs) have been developed to predict material properties such as permittivity, permeability, and conductivity [8],[45]. While EMTs have limitations, they are powerful tools that agree well with experimental results in various applications under the proper conditions [3]. From an electrical taper perspective, it is conceivable to leverage the concept of EMTs and apply them for extracting the necessary volume fractions that one would need along a transmission line. Motivated by this, we return to (17) and express it in terms of the ratio of the dielectric properties along the length of the line for an exponential taper. For the linear case, this is given by

$$\frac{\mu_r(x)}{\epsilon_r(x)} = \left(\frac{2\pi Z_i e^{\pm kx}}{\ln(b/a)}\right)^2 \left(\frac{\epsilon_o}{\mu_o}\right) \tag{30}$$

Equation (30) allows the designer to determine the ratio of the permeability to permittivity along the line for a given geometry and taper ratio. After tabulating the necessary ratios, the

designer may utilize an EMT to predict the volume fraction of the composite that is needed for that ratio. Table 5 summarizes several of the EMTs from the literature.

Here, we consider the classical EMT known as the Maxwell Garnett (MG) formula for spheres, which has been widely used for assessing a material's electromagnetic properties [50]. The true motivation for using the MG rule is the ease of extracting the necessary volume fraction. We can express the permittivity ϵ_r and permeability μ_r as

$$\epsilon_r = \epsilon_e + 3f\epsilon_e * \frac{\epsilon_i - \epsilon_e}{\epsilon_i + 2\epsilon_e - f(\epsilon_i - \epsilon_e)} \tag{31}$$

$$\mu_r = \mu_e + 3f\mu_e * \frac{\mu_i - \mu_e}{\mu_i + 2\mu_e - f(\mu_i - \mu_e)} \tag{32}$$

Table 5 Common effective medium theories(EMTs) used in literature

Ref.	Mixing Law	Equation
[46]	Maxwell-Garnett	$\epsilon_{eff} = \epsilon_e + 3f\epsilon_e \frac{\epsilon_i - \epsilon_e}{\epsilon_i + 2\epsilon_e - f(\epsilon_i - \epsilon_e)}$
[48]	Lichtenecker	$\log \epsilon_{eff} = f \log \epsilon_i + (1-f) \log \epsilon_e$
[47]	Bruggeman	$(1-f)\frac{\epsilon_e - \epsilon_{eff}}{\epsilon_e + 2\epsilon_{eff}} + f\frac{\epsilon_i - \epsilon_{eff}}{\epsilon_i + 2\epsilon_{eff}} = 0$
[45]	Coherent Potential	$\epsilon_{eff} = \epsilon_e + f(\epsilon_i - \epsilon_e)\frac{3\epsilon_{eff}}{3\epsilon_{eff} + (1-f)(\epsilon_i - \epsilon_e)}$
[49]	Looyenga	$\epsilon_{eff}^{1/3} = (1-f)\epsilon_e^{1/3} + f\epsilon_i^{1/3}$

where f is the volume fraction, ϵ_e and μ_e are the permittivity and permeability of the host, respectively, ϵ_i and μ_i are the permittivity and permeability of the inclusions, respectively. For a

given initial impedance Z_i and taper ratio Z_L/Z_i, we obtain the necessary volume fraction by substituting (31) and (32) into (30) and solving for *f* to obtain

$$f_{MG} = \frac{(\mu_e\alpha + A\beta + \Gamma + \sqrt{\Delta + \Lambda})}{4(\epsilon_e - \epsilon_i)(A\epsilon_e - \mu_e)(\mu_e - \mu_i)} \tag{33}$$

where, for notational convenience, we have defined

$$\alpha = 2(\epsilon_e + 2\epsilon_i)\mu_e - (5\epsilon_e + \epsilon_i)\mu_i, \tag{34}$$

$$A = \left(\frac{2\pi Z_i e^{\pm kx}}{\ln(b/a)}\right)^2 \left(\frac{\epsilon_o}{\mu_o}\right), \tag{35}$$

$$\beta = \epsilon_e(5\mu_e + \mu_i), \tag{36}$$

$$\Gamma = 2\epsilon_e(\mu_e + 2\mu_i), \tag{37}$$

$$\Delta = \sqrt{(8(\epsilon_e - \epsilon_i)(2\epsilon_e + \epsilon_i)(-A\epsilon_e + \mu_e)^2(\mu_e - \mu_i)(2\mu_e + \mu_e)}, \tag{38}$$

and

$$\Lambda = (\mu_e(-2(\epsilon_e + 2\epsilon_i)\mu_e + (5\epsilon_e + \epsilon_i)\mu_e) + A\epsilon_e(-\epsilon_i(5\mu_e + \mu_i) + 2\epsilon_e(\mu_e + 2\mu_i)))^2 \tag{39}$$

Equation (33) is valid for the volume fraction needed for a single inclusion linear composite whose permittivity and permeability vary with volume loading. Therefore, knowing line dimensions and host material properties, one can predict the necessary volume fraction needed along the line to achieve an exponential taper for various taper ratios. A host of parametric studies can be performed,

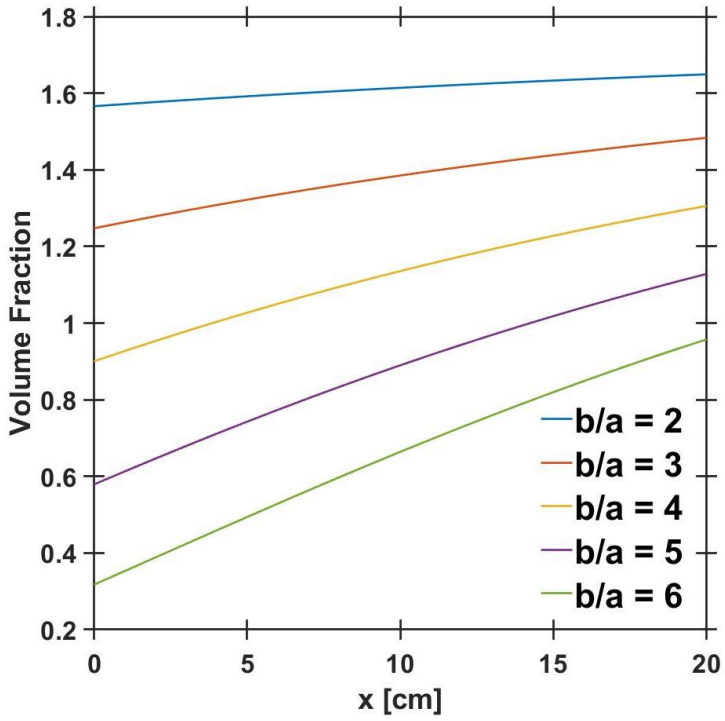

Figure 21 The necessary volume loading along a line for various of inner to outer diameter (*b*/*a*) for an exponential taper from 75 Ω to 100 Ω taper using (33). The volume fraction is allowed the vary along the line, while *b*/*a* is constant along the line, unlike a physically tapered line, where *b*/*a* varies.

such as investigating the effects of changing the ratio of inner and outer diameter but fixing them for the total line length, the total length of the line, and the permittivity and permeability of the host and/or inclusion. As a brief example, we consider a taper from 75 to 100 Ω using a linear material encased in PDMS. We set $\mu_e = 1$, $\mu_i = 5$, $\epsilon_e = 2.7$, $\epsilon_i = 5.5$, and the total line length to 20 cm. Using (33), we can assess the necessary volume fractions needed for this material for different values of *b*/*a*. Figure 21 shows the conditions of b/a where the required volume fraction is not physically realizable (e.g., $f < 0$ or $f > 1$).

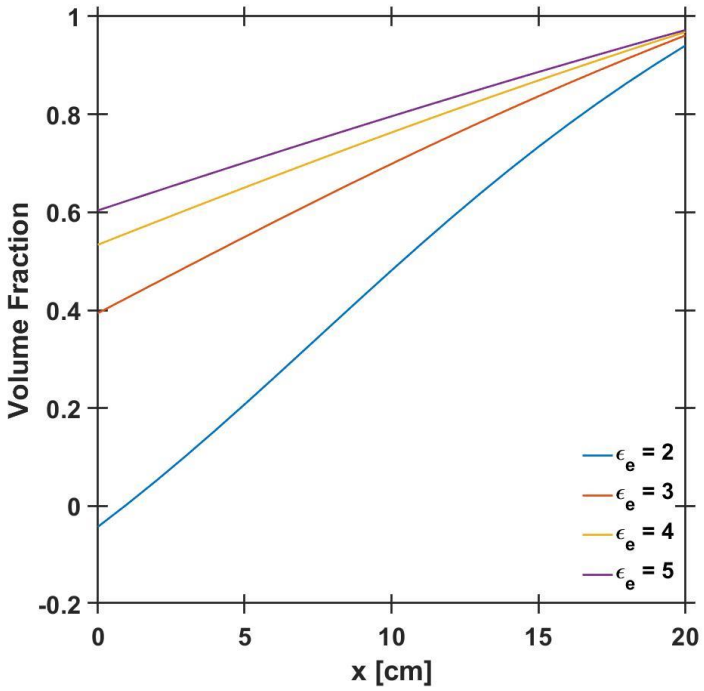

Figure 22 The effect of changing the host permittivity for a 75-100 Ω taper for a 20 cm long transmission line.

For the same taper mentioned above, we can also assess the impact of changing the host encapsulation media. Figure 22 shows that fixing the ratio of b/a = 6 and allowing the permittivity of the host media to vary from 2-5 shows that increasing the permittivity of the host increases the inclusion volume fraction needed for the taper. Since the taper ratio in this scenario is positive, this makes sense since the impedance is inversely proportional to the permittivity. Therefore, we need a greater volume fraction to sufficiently change the permeability to achieve the desired ratio.

Theoretically, we can extend the above analysis to the nonlinear permeability case by including the nonlinear term from (23) into (35). However, this again would require a constitutive relation describing the current as a function of position or the assumption that each section is electrically small. Considering that our composite permeability did not exhibit statistically significant nonlinearity with respect to the magnetic field until reaching volume fractions of 15%, we conjecture that (33) will be valid for volume fractions <15% or at low power where the current dependence is small. In future studies, we will develop the constitutive relation for the current as a function of position to substitute into (35) to develop an equation to predict behavior over the entire range of volume fractions for nonlinear materials rather than just the small volume fractions

of nonlinear materials. We also intend to replace the current dependence of the permeability with fits that are more accurate and relevant to our observed parameter measurements, such as the hyperbolic tangent function. In conjunction with this, we plan to manufacture an electrically tapered linear and nonlinear transmission line to show the feasibility of this concept using the manufacturing procedures and materials described in chapter 3.

5. CONCLUSIONS AND FUTURE WORK

This research focused on experimentally measuring the nonlinear relative permeability and magnetic loss tangents of composites for nonlinear transmission lines by subjecting them to external magnetic fields and measuring their S-parameters using a network analyzer. The S-parameters were then imported into commercial software to extract the permeability using the Polynomial Fit Transmission and Reflection model. This model was selected because it can extract the material properties from magnetic samples.

The composites were manufactured using a two-part silicon polymer base called PDMS and various volume fractions of a ferroelectric material, barium strontium titanate and a ferrimagnetic material, nickel zinc ferrite. Ferrimagnetic and ferroelectric materials are well-known for their nonlinear behavior with respect to magnetic and electric fields; however, the characterization of their nonlinearity highly depends on frequency, field strength, volume loading of material and manufacturing procedure. Therefore, it is paramount to experimentally characterize the composite's nonlinear properties, such as its permeability in the case of this thesis, before one can efficiently implement it into a system design. The ultimate goal of this research is to utilize these composites in future NLTL designs guided by the results of this thesis.

The results of the experiment suggest that the permeability is strongly coupled to the bias field strength, frequency, and volume fraction as initially expected. When investigating the impact of frequency, we observed that the composite permeability at applied fields of $H \lesssim 100$ kA/m decreased. However, the decrease did not become statistically significant until NZF volume loadings exceeded 15%. When $H \gtrsim 100$ kA/m, the permeability of the composite was insensitive to frequency.

We next investigated the impact of the applied field on the composite for each individual frequency. In general, at 1 and 2 GHz, field strengths of greater than 100 kA/m were needed to induce statistically significant changes. At 3 and 4 GHz, the only insignificant changes occurred when comparing 45.49 ± 2.06 kA/m to 137.58 ± 9.07 kA/m and 0 to 171.18 ± 5.07 kA/m which is a result of the profile the permeability had. Unlike at 1 and 2 GHz, the permeability increased at $H \lesssim 100$ kA/m at 3 and 4 GHz. This observation had some implications on NLTL design which were discussed in Chapter 3. Volume fractions of 15% NZF were also necessary to induce statistical significance in the change of permeability with respect to the magnetic field.

The impact of adding a nonlinear dielectric like BST on an NZF composite was investigated. The data suggests that BST in small volume fractions does not alter the permeability in a statistically significant way. Of greater importance was the suppression of magnetic loss tangents by adding BST. This was an unexpected result, although Ref. [15] also exhibited this phenomenon. Also of interest is the high dielectric constant of BST, which substantially increases a composite's permittivity. From a pulsed power perspective, this is advantageous for preventing breakdown between the inner and outer conductor.

The dependence of the permeability on volume loading was also explored. In general, a change of 10% in NZF was required to induce statistically significant changes in the permeability with respect to the volume loading. Moreover, the concept of varying volume loading for altering effective composite properties motivated us to develop a theory for tapering transmission lines for impedance matching in Chapter 4. Such a taper would bypass the complicated geometries and cumbersome manufacturing processes of geometrical tapering by instead implementing an electrical taper.

The electrical taper would consist of discrete sections of coaxial line with fixed inner and outer radius, gradually linked together to achieve the appropriate impedance. In chapter 4, it was also shown that allowing the permittivity and permeability to vary exponentially with distance results in an exponential impedance profile. Leveraging this, a process for determining the total line length and length of each section was determined by looking at the reflection coefficient. A nonlinear term was then added to the permeability to make it current dependent thus mimicking the behavior of our NZF where the permittivity and permeability scaled with volume loading but the permeability was nonlinear. Similar steps were followed to determine the reflection coefficient for the nonlinear impedance although without a constitutive relation for current, several assumptions had to be made. The assumptions require that each section must be sufficiently small such that the current within the section remains constant; this also implies the line be lossless.

Effective medium theories were then implemented to predict the necessary volume fraction of material that one would need to achieve such a taper. The Maxwell Garnett rule was used as it was the most straight forward for extracting the necessary volume fraction but the analysis is not limited to that EMT only. A brief example looking at the impact of changing the ratio of the inner and outer diameter and host permittivity was given.

The electrical taper is not limited to only nonlinear transmission lines. In practice, it may also be implemented in linear transmission lines and conceivably in microstrip systems. Further developing the theory of nonlinear tapers will require developing a constitutive relation for the current as a function of position. Other sigmoidal expressions, such as hyperbolic tangent and secant functions, have been used to express the current and/or voltage dependence of a ferrite/ferroelectric in the literature and typically give better fitting results, albeit with some additional mathematical complication. This thesis applied a linear approximation for a preliminary calculation because it was mathematically convenient while still yielding a reasonable first order approximation for composites with low volume fractions of nonlinear material or low frequencies.

Future studies will involve implementing these composites in NLTLs and testing them with various pulsed power drivers such as Blumlein generators and inductive adders; the results provided here will provide a guide for composite development and parameter estimation for system design. In conjunction with this, we plan to continue to investigate and develop the theory for nonlinear tapers and inevitably implement them in a modular NLTL system for HPM applications.

REFERENCES

[1] K. M. Noel, R. D. Curry, A. M. Pearson, and K. A. O'Connor, "The dielectric strength of high frequency metamaterial composites," in *Proc. 20th IEEE Pulsed Power Conf.*, 2015, pp. 1–3.

[2] R. D. Curry, A. M. Pearson, K. M. Noel, and S. Mounter, "Development of Metamaterial Composites for Compact High Power Microwave Systems and Antennas," Columbia, MO, 2016.

[3] A. L. Garner, G. J. Parker, and D. L. Simone, "A semi-empirical approach for predicting the performance of multiphase composites at microwave frequencies," *IEEE Trans. Dielectr. Electr. Insul.*, vol. 23, pp. 1126-1134, 2016.

[4] D.V. Reale, "Coaxial Ferrimagnetic Based Gyromagnetic Nonlinear Transmission Lines as Compact High Power Microwave Sources," Ph.D. Dissertation in Electrical Engineering, Texas Tech University, Dec. 2013.

[5] J. Benford, J. A. Swegle, "High Power Microwaves Third Edition," Taylor & Francis Group, 2016.

[6] A.S. Gilmour, "Kylstrons, Traveling Wave Tubes, Magnetrons, Cross-Field Amplifiers and Gyrotrons," Archetch House, 2011.

[7] J. W. Bragg, J. C. Dicken, A. A Neuber, "Ferrimagnetic nonlinear transmission lines as high-power microwave sources," *IEEE Trans.Plasma Sci.,* vol. 41, pp. 232-237, 2013.

[8] X. Zhu, "Assesing Effective Medium Theories for Designing Composites for Nonlinear Transmission Lines," A Thesis in Nuclear Engineering, Purdue University, 2019.

[9] J. W. B. Bragg, J. C. Dickens, and A. A. Neuber, "Material selection considerations for coaxial, ferrimagnetic-based nonlinear transmission lines," *J. Appl. Phys*., vol. 113, 2013, Art. no. 064904.

[10] A. J. Fairbanks, A. M. Darr, and A. L. Garner, "A review of nonlinear transmission line system design," *IEEE Access,* vol. 8, pp. 148606 – 148621, 2020.

[11] L. P. S. Neto, J. O. Rossi, J. J. Barroso, and E. Schamiloglu, "Hybrid nonlinear transmission lines used for RF soliton generation," *IEEE Trans. Plasma Sci.*, vol. 46, no. 10, pp. 3648–3652, Oct. 2018.

[12] E. Afshari and A. Hajimiri, "Nonlinear transmission lines for pulse shaping in silicon," *IEEE J. Solid-State Circuits,* vol. 40, no. 3, pp. 744–752, Mar. 2005.

[13] N. S. Kuek, A. C. Liew, E. Schamiloglu, and J. O. Rossi, ‘‘Pulsed RF oscillations on a nonlinear capacitive transmission line,’’ *IEEE Trans. Dielectr. Electr. Insul*., vol. 20, no. 4, pp. 1129–1135, Aug. 2013.

[14] J. O. Rossi, L. P. Silva, J. J. Barroso, F. S. Yamasaki, and E. Schamiloglu, ‘‘Overview of RF generation using nonlinear transmission lines,’’ in Proc. IEEE Pulsed Power Conf. (PPC), May 2015, pp. 1–6.

[15] J. A. Schrock, B. W. Hoff, D. H. Simon, S. L. Heidger, P. Lepell, J. Gilbrech, H. Wood, and R. Richter-Sand, ‘‘Spatially dispersive nonlinear transmission line experimental performance analysis,’’ *IEEE Trans. Dielectr. Electr. Insul*., vol. 26, no. 2, pp. 412–415, Apr. 2019.

[16] L. R. Raimundi, J. O. Rossi, E. G. L. Rangel, L. C. Silva, E. Schamiloglu, and L. P. S. Neto, ‘‘RF generation at 200 MHz using a SiC Schottky diode lumped NLTL,’’ in Proc. IEEE Int. Power Modulator High Voltage Conf. (IPMHVC), Jun. 2018, pp. 473–476.

[17] M. R. Ul’maskulov, S. A. Shunailov, K. A. Sharypov, M. I. Yalandin, V. G. Shpak, M. S. Pedos, and S. N. Rukin, ‘‘Coherent summation of radiation from four-channel shock-excited RF source operating at 4 GHz and a repetition rate of 1000 Hz,’’ *IEEE Trans. Plasma Sci*., vol. 45, no. 10, pp. 2623–2628, Oct. 2017.

[18] D. V. Reale, J.-W.-B. Bragg, N. R. Gonsalves, J. M. Johnson, A. A. Neuber, J. C. Dickens, and J. J. Mankowski, ‘‘Bias-field controlled phasing and power combination of gyromagnetic nonlinear transmission lines,’’ *Rev. Sci. Instrum*., vol. 85, no. 5, May 2014, Art. no. 054706.

[19] F. S. Yamasaki, J. O. Rossi, J. J. Barroso, and E. Schamiloglu, “Operation of a gyromagnetic line at low and high voltages with simultaneous axial and azimuthal biases,” *IEEE Trans. Plasma Sci.*, vol. 46, no. 7, pp. 2573–2581, Jul. 2018.

[20] D. J. Griffiths, “Introduction to Electrodynamics Fourth Edition,” Pearson Education Inc., 2013.

[21] J. Stohr and H.C. Seigemann, “Magnetism,” Springer Berlin Hiedelberg, 2006.

[22] R. M. White, “Quantum Theory of Magnetism,” Springer, 2006.

[23] J. Gaudet, E. Schamiloglu, J. O. Rossi, C. J. Buchenauer, and C. Frost, “Nonlinear transmission lines for high power microwave applications - A survey,” *Proc. 2008 IEEE Int. Power Modul. High Volt. Conf. PMHVC*, pp. 131–138, 2008.I. S. Jacobs and C. P. Bean, “Fine particles, thin films and exchange anisotropy,” in *Magnetism*, vol. III, G. T. Rado and H. Suhl, Eds. New York: Academic, 1963, pp. 271-350.

[24] E. G. L. Rangel, J. O. Rossi, J. J. Barroso, F. S. Yamasaki, and E. Schamiloglu, “Practical constraints on nonlinear transmission lines for RF generation,” *IEEE Trans. Plasma Sci.*, vol. 47, no. 1, pp. 1000–1016, Jan. 2019.

[25] K. M. Noel, A. M. Pearson, R. D. Curry, and K. A. O. Connor, "High frequency properties of high voltage barium titanate-ferrite multiferroic metamaterial composites," *IEEE Trans. Dielectr. Electr. Insul.*, vol. 23, no. 5, pp. 2965–2969, 2016.

[26] A. L. Garner, G. J. Parker, and D. L. Simone, "Predicting effective permittivity of composites containing conductive inclusions at microwave frequencies," *AIP Adv.*, vol. 2, no. 3, Sep. 2012, Art. no. 032109.

[27] A. L. Garner, G. J. Parker, and D. L. Simone, "Accounting for conducting inclusion permeability in the microwave regime in a modified generalized effective medium theory," *IEEE Trans. Dielectr. Electr. Insul.*, vol. 22, no. 1, pp. 2064–2072, 2015.

[28] Z. Wang, J. K. Nelson, J. Miao, R. Linhardt, L. S. Schadler, H. Hillborg, and S. Zhao, "Effect of high aspect ratio filler on dielectric properties of polymer composites: a study on barium titanate fibers and graphene platelets," *IEEE Trans. Dielectr. Electr. Insul.*, vol. 19, no. 3, pp. 960–967, Jun. 2012.

[29] X. Wen, S. J. Kelly, J. S. Andrew, and D. P. Arnold, "Nickel-zinc ferrite/permalloy ($Ni_{0.5}Zn_{0.5}Fe_2O_4$/Ni-Fe) soft magnetic nanocomposites fabricated by electro-infiltration," *AIP Adv.*, vol. 6, 2016, Art. no. 056111.

[30] J. T. Allanson, "The permeability of ferromagnetic materials at frequencies between 10^5 and 10^{10} c/s," *J. Inst. Electr. Eng. - Part III Radio Commun. Eng.*, vol. 92, no. 20, pp. 247–255, 1945.

[31] R. E. Collin, " Foundations of Microwave Engineering Second Edition," Wiley & Sons, 2001.

[32] S. Ramo, J. R. Whinnery, T. Van Duzer, "Fields and Waves In Communication Electronics Third Edition," Wiley & Sons, 1994.

[33] A. H. Wing and J. Eisenstein, "Single- and double-stub impedance matching," *J. Appl. Phys.*, vol. 15, no. 8, pp. 615-622, 1944.

[34] M. Chongcheawchamnan, S. Patisang, S. Srisathit, R. Phromloungsri, and S. Bunnjaweht, "Analysis and design of a three-section transmission line transformer," *IEEE Trans. Microw. Theory Tech.*, vol. 53, pp. 2458-2462, 2005.

[35] R. E. Collin, "Design of wide-band multisection quarter wave transformers," *Proc. IRE*, vol. 43, no. 2, pp. 179-185, 1955.

[36] H. J. Riblet, "General synthesis of quarter-wave impedance transformers," *IRE Trans. Microw. Theory Tech.*, vol. 5, no. 1, pp. 36-43, Jan. 1957.

[37] L. Vegni, F. Urbani, and A. Toscano, "Exponentially tapered non-uniform transmission lines," *IEEE Trans. Magn.*, vol. 33, pp. 1492-1495, 1997.

[38] D. M. Pozar, "Microwave Engineering 4^{th} ed," Wiley & Sons, 2012.

[39] H. Altschnfer, J. Fox, and A. C. Lynch, “Impedance transformation equations for exponential, cosine-squared, and parabolic tapered transmission lines,” *IEEE Trans. Microw. Theory Tech*., vol. 29, pp. 67-68, 1981.

[40] V. Ramachandran, “Impedance matching by uniform transmission lines,” *IETE J. Educ*., vol. 3, pp. 70-81 1962.

[41] P. K. Verma, R. Kumar and M. Singh, "Design and simulation of dielectric tapered rod as feed for dielectric lens antenna at 140 GHz," *2008 International Conference on Recent Advances in Microwave Theory and Applications*, Jaipur, 2008, pp. 233-235, doi: 10.1109/AMTA.2008.4763117.

[42] C. Liu and C. Chen, "A UWB three-layer dielectric rod antenna with constant gain, pattern and phase center," *IEEE Trans. Ant. Propag.*, vol. 60, no. 10, pp. 4500-4508, Oct. 2012.

[43] C. C. Che, K. Rama Rao, and R. Lee, “A tapered-permittivity rod antenna for ground penetrating radar applications,” *J. Appl. Geophys*., vol. 47, pp. 309-316, 2001.

[44] J. Yi, G. P. Piau, A. De Lustrac, and S. N. Burokur, “Electromagnetic field tapering using all-dielectric gradient index materials,” *Sci. Rep*., vol. 6, 2016, Art. no. 30661.

[45] A. H. Sihvola, “*Electromagnetic Mixing Formulas and Applications,”* London, U.K.: IET, 1999.

[46] J. C. Maxwell Garnett, “Colours in metal glasses and in metallic films,” *Philos. Trans. R. Soc., London, Ser. A.*, vol. 203, pp. 385-420, 1904.

[47] D. A. G. Bruggeman, “Calculation of various physics constants in heterogeneous substances I Dielectric constants and conductivity of mixed bodies from isotropic substances,” *Ann. Phys*., vol. 24, no. 7, pp. 636-664, 1935.

[48] K. Lichtenecker, “Dielectric constant of natural and synthetic mixtures,” *Phys. Z,* vol. 27, pp. 115-158, 1926.

[49] H. Looyenga, “Dielectric constants of heterogeneous mixtures,” *Physica,* vol. 31, no. 3, pp. 401–406, Mar. 1965.

[50] V. A. Markel, “Introduction to the Maxwell Garnett approximation: tutorial,” *J. Opt. Soc. Amer. A, Opt. Image Sci.*, vol. 33, no. 7, pp. 1244–1256, 2016.

[51] S. A. P. Rizvi and R. A. A. Khan, "Klopfenstein tapered 2–18 GHz microstrip balun," *Proceedings of 2012 9th International Bhurban Conference on Applied Sciences & Technology (IBCAST)*, Islamabad, 2012, pp. 359-362, doi: 10.1109/IBCAST.2012.6177579.

[52] S. Chen and Z. Liang, "The impedance matching analysis on different tapered line function," *2011 4th IEEE International Conference on Broadband Network and Multimedia Technology*, Shenzhen, 2011, pp. 620-623, doi: 10.1109/ICBNMT.2011.6156009.

[53] H. Ikezi, J. S. DeGrassie, and J. Drake, "Soliton generation at 10 MW level in the very high frequency band," *Appl. Phys. Lett*., vol. 58, no. 9, pp. 986–987, Mar. 1991.

[54] S. Hollung, J. Stake, L. Dillner, M. Ingvarson, and E. Kollberg, "A distributed heterostructure barrier varactor frequency tripler," *IEEE Microw. Guided Wave Lett*., vol. 10, no. 1, pp. 24–26, Jan. 2000.

[55] X. Melique et al., "12% efficiency and 9.5 dBm output power from InP-based heterostructure barrier varactor triplers at 250 GHz," in IEEE MTT-S Int. Microw. Symp. Dig., Anaheim, CA, USA, vol. 1, Jun. 1999, pp. 123–126

[56] F. S. Yamasaki, J. O. Rossi, J. J. Barroso and E. Schamiloglu, "Operation of a gyromagnetic line at low and high voltages with simultaneous axial and azimuthal biases," *IEEE Trans. Plasma Sci.*, vol. 46, no. 7, pp. 2573-2581, Jul. 2018.

[57] M. Tokuyama and H. Ohtagaki, ''Chaos in a series circuit with a nonlinear capacitor and a nonlinear inductor,'' *Electr. Eng. Jpn.*, vol. 150, no. 2, pp. 35–42, Jan. 2005.

[58] N. S. Kuek, A. C. Liew, E. Schamiloglu, and J. O. Rossi, ''RF pulse generator based on a nonlinear hybrid line,'' *IEEE Trans. Plasma Sci*., vol. 42, no. 10, pp. 3268–3273, Oct. 2014.

[59] L. Yan, J. Wang, Y. Ye, Z. Hao, Q. Liu, F. Li, "Broadband and thin microwave absorber of nickel-zinc ferrite/carbonyl iron composite," *J. Alloys. Compd*., vol. 487, pp. 708-711, 2009.

[60] A.F. Ahmed, Z. Abbas, S. J. Obaiys, and D. M. Abdalhadi, "Improvement of dielectric, magnetic and thermal properties of OPEFB fibre–polycaprolactone composite by adding Ni–Zn ferrite," *Polymers*, vol. 9, 2017, Art. no. 12.

[61] A. M. A. Henaish, M. Mostafa, B. I. Salem, and O.M. Hemeda, "Improvement of magnetic and dielectric properties of magnetoelectric BST-NCZMF nano-composite," *Phase Transit*., vol. 93, pp. 470-490, 2020.

[62] K. N. Rozanov, Z. W. Li, L.F. Chen, and M. Y. Koledinsteva, "Microwave permeability of Co_2Z composites," *J. Appl. Phys*., vol. 97, no. 1, 2005, Art. no. 013905.

[63] P. Singh, V. K. Babbar, A. Razdan, T. K. Puri, and T.C. Goel, "Complex permittivity, permeability, and X-band microwave absorption of CaCoTi ferrite composite," *J. Appl. Phys*., vol. 87, no. 9, pp. 4362-4366, 2000.

[64] J. S. Ghodake, R. C. Kambale, T. J. Shinde, P. K. Maskar, and S.S Suryvananshi, “Magnetic and microwave absorbing properties of Co^{2+} substituted nickel-zinc-ferrites with emphasis on initial permeability studies,” *J. Magn. Magn. Mater*., vol. 401, pp. 938-942, 2016.